Experimental Analysis of hill-climbing MPPT algorithms under low irradiance levels

Vibhu Jately; Brian Azzopardi; Jyoti Joshi; Balaji Venkateswaran V; Abhinav Sharma; Sudha Arora

Published in:
Renewable and Sustainable Energy Reviews

Publication date:
11 July 2021

Document Version
Peer-reviewed version

Citation for published version (IEEE format):
V. Jately, B. Azzopardi, J. Joshi, B. Venkateswaran V, A. Sharma, S. Arora, "Experimental Analysis of hill-climbing MPPT algorithms under low irradiance levels," *Renewable and Sustainable Energy Reviews*, Vol. 150, pp. 111467, 2021. doi: 10.1016/j.rser.2021.111467.

Experimental Analysis of Hill-Climbing MPPT Algorithms under Low Irradiance Levels

Vibhu Jately [a*], Brian Azzopardi [a], Jyoti Joshi [b], Balaji Venkateswaran V [c], Abhinav Sharma [d], Sudha Arora [b]

[a*] *MCAST Energy Research Group (MCAST Energy), Institute of Engineering and Transport, Malta College of Arts, Science and Technology (MCAST), Triq Kordin, Paola PLA 9032, Malta*

[b] *Department of Electrical Engineering, G. B. Pant University of Agriculture and Technology, Pantnagar, 263145, India*

[c] *School of Technology, Woxsen University, Hyderabad, Telangana, 502345, India*

[d] *Department of Electrical and Electronics Engineering, University of Petroleum and Energy Studies, Dehradun 248007, India*

[*] Corresponding author.

Email Addresses: vibhujately@gmail.com (V. Jately), brian.azzopardi@mcast.edu.mt (B. Azzopardi), jjyotij25@gmail.com (J. Joshi) balajivenkateswaran.v@gmail.com (Balaji Venkateswaran V), abhinavgbpuat@gmail.com (A. Sharma), arora.sudha@gmail.com (S. Arora)

Abstract: Adaptive hill-climbing MPPT algorithms have superior performance as opposed to their conventional counterparts under medium-high irradiance. However, the performance of these hill-climbing algorithms remains mostly unknown under low irradiance condition. The low irradiance conditions are prominent in tropical countries during rainy seasons and niche PV applications. Additionally, several thin-film photovoltaic (PV) technologies have better efficiency under low irradiance conditions. Hence, the optimum operation of MPPT algorithms under low irradiance conditions is vital. In the real-time implementation, MPPT algorithms can fail to detect the incremental changes in voltage and current under low irradiance conditions. Hence, analog to digital converter (ADC) resolution becomes a critical constraint that governs the performance of hill-climbing (HC) MPPT algorithms. This work entails a detailed calculation to determine the perturbation step-sizes of the MPPT algorithms under a wide range of irradiance. Two distinct perturbation step-sizes are determined corresponding to the minimum and optimum change in voltage and current due to perturbation, that is sensed by the ADC. The authors also defined a general expression to determine the optimum digitized step-size for duty-based perturb and observe algorithm under low irradiance condition. This expression is formulated by considering the resolution of the ADC and the desirability of keeping the power oscillations at an acceptable level. Finally, the performance of eight hill-climbing algorithms for two distinct step-sizes is analyzed on a small-scale experimental prototype under both uniform and sudden changes in low values of irradiance. The statistical analysis validates that the adaptive HC drift-free MPPT algorithm outperforms other HC algorithms when implemented with the optimum perturbation step-size under low irradiance conditions.

Keywords: *Hill-climbing, MPPT, Perturb and Observe, perturbation step-size, ADC, Incremental conductance*

List of Abbreviations

ADC	Analog to Digital Converter	GAF-VPF	Gaussian–Arctangent Function Variable Perturbation Frequency
AHC	Adaptive Hill-Climbing	I&T	Irradiance & Temperature
AI	Artificial Intelligence	MPP	Maximum power point
ANN	Artificial Neural Network	MPPT	Maximum power point tracking
ASF	Adaptive Scaling Factor	OSS	Optimum step-size
BST	Bisection Search Theorem	OC	Open circuit
C/A-P&O	Conventional/Adaptive Perturb and Observe	PI	Proportional Integral
C/A-INC	Conventional/Adaptive Incremental Conductance	PSO	Particle swarm optimization
C/A-DF	Conventional/Adaptive Drift-Free	PV	Photovoltaic
C-INR	Conventional Incremental Resistance	SA	Simulated Annealing
CCL	Current Control Loop	SC	Short circuit
CHC	Conventional Hill-Climbing	SM-ESC	Sliding-mode extremum seeking control

CSAM	Current sensor-less method with auto-modulation	SS	Steady-state
CV	Constant voltage	SSS	Suboptimal step-sizes
DCPA	Duty-cycle perturbations adaptation	STC	Standard Test Condition
ESC	Extremum seeking control	TG	Temperature gradient
FLC	Fuzzy logic control	VCL	Voltage Control Loop

Nomenclature

I_{PV}	PV current	G	Irradiance
V_{PV}	PV voltage	T	Temperature
P_{PV}	PV power	$D(k)$	duty at k^{th} iteration
V_{MPP}	Voltage at MPP	$D(k\text{-}1)$	duty at $(k\text{-}1)^{th}$ iteration
I_{MPP}	Current at MPP	ΔD	duty step-size
ΔI	Current step-size	ΔV	Voltage step-size
P_{MPP}	Power at MPP	$P(k\text{-}1)/P(k\text{-}2)$	PV power at $(k\text{-}1)^{th}/(k\text{-}2)^{th}$ iteration
V_{OC}	Open-circuit voltage	ΔD_{max}	maximum step-size in duty
I_{SC}	Short-circuit current	dV_{max}	change in voltage corresponding to ΔD_{max}
$V_{ref}(k)$	Reference voltage at k^{th} iteration	dP_{max}	change in power corresponding to ΔD_{max}
$V(k-1)$	PV voltage at $(k\text{-}1)^{th}$ iteration	ΔV_{max}	maximum step-size in voltage
$I_{ref}(k)$	Reference current at k^{th} iteration	ΔI_{max}	maximum step-size in current
$I(k-1)$	PV current at $(k\text{-}1)^{th}$ iteration	N_C	Number of solar cells
L	Inductance	β_{OC}	Open-circuit temperature coefficient
C	Capacitance	α_{SC}	Short-circuit temperature coefficient
R	Load resistance	dV_{min}	Minimum voltage sensing ability of the microcontroller due to perturbation
D	Duty	dI_{min}	Minimum current sensing ability of the microcontroller due to perturbation
dV_{opt}	Optimum change in voltage sensed by the microcontroller due to perturbation	dI_{opt}	Optimum change in current sensed by the microcontroller due to perturbation
$D_{mpp(G)}$	Duty cycle at MPP at G	$V_{mpp(G)}$	Voltage at MPP at G
$I_{mpp}(G)$	Current at MPP at G	ΔD_{opt}	Optimum duty cycle
$\tilde{V}_{PV}$	Small perturbations in PV voltage	$\tilde{d}$	Small perturbations in duty
t_{ss}	Steady-state response time	$\widetilde{I_{PV}}$	Small perturbations in PV current

1. Introduction

Annual Energy Outlook (AEO2019) has reported that at the present rate of consumption, all the non-renewable sources of energy like coal, oil, and uranium would deplete within a few decades [1]. Besides being exhaustible, these forms of energy are adding to the already beleaguered state of environmental pollution. This situation has prompted various government agencies and industries to come up with new policies and to look for new cleaner forms of energy resources that are renewable. Among these sources, solar energy is becoming the most reliable one, as it is profusely available [2].

Nowadays, PV systems are built and used with output power ranging from a few milli-watts in scientific calculators to MWs in solar farms for residential/industrial applications [3]. Medium-large scale

PV systems require power converters (inverter, chopper) depending upon the nature of the load. These units not only help in achieving the desired voltage and frequency of operation but also extract maximum power from PV modules [4]. The power converter, along with an MPPT algorithm, is a MPPT controller, which is a crucial component in most PV systems. This controller tries to find MPP, which lies in the curved region of the current-voltage (I-V) characteristics of a photovoltaic module, shown in Fig. 1. MPP tracking is the continuous process of finding this MPP in the non-linear region of the I-V curve. This tracking becomes complex in nature when the MPP needs to be located on a changing I-V characteristic under variation in irradiance (G), temperature (T), and load [5]. Several MPPT algorithms have been published that work well under uniform and rapidly changing meteorological conditions [6 – 17].

Among the existing MPPT techniques, hill-climbing algorithms are extensively used in both research and industrial applications because they are array independent, efficient and easily implemented in an inexpensive controller. A brief classification of the most commonly used hill-climbing algorithms is shown in Fig. 2.

Both C-P&O and C-INC algorithms utilize knowledge of the power-voltage (P-V) curve, whereas C-INR uses knowledge of the power-current (P-I) curve to speculate the sign of the next perturbation. Although these classical algorithms are efficient, these suffer from a quid pro quo between their dynamic and steady-state (SS) response. A large perturbation step-size improves the dynamic response but results in inadequate SS response, whereas a small perturbation step does refine the SS response but slows down the tracking process.

The adaptive versions of these HC algorithms, i.e., Adaptive P&O (A-P&O), Adaptive INC (A-INC), and Adaptive INR (A-INR) are more popular as they try to create a balance between this trade-off. These algorithms adaptively increase or decrease the perturbation step-size based on the region of the operating point on the power curve [18 – 20].

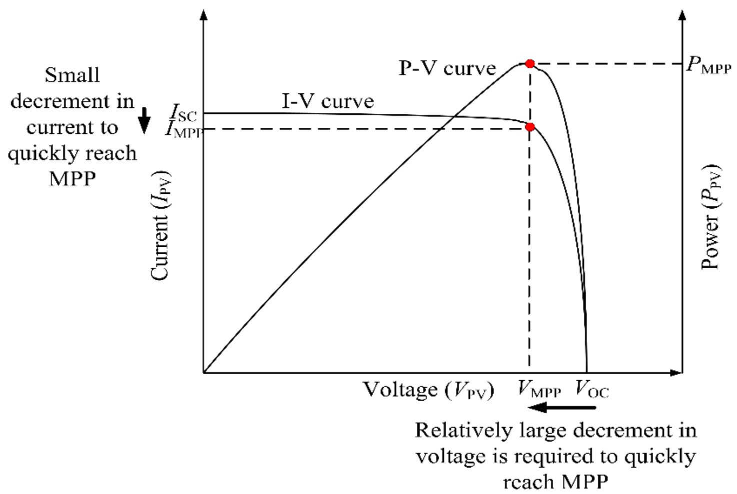

Fig. 1. I-V and P-V plot of PV module

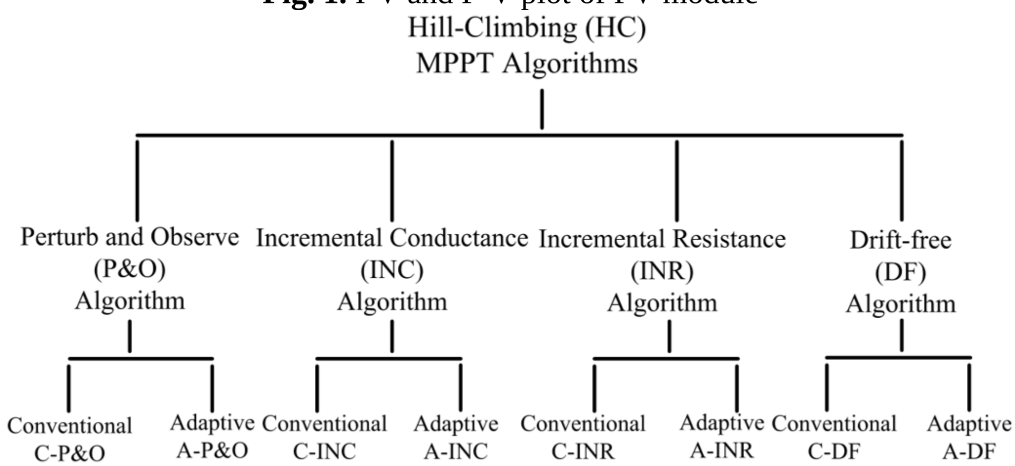

Fig. 2. Classification of commonly used Hill-Climbing MPPT Algorithms

Moreover, these conventional and adaptive algorithms also lose their MPP tracking capability which results in power losses under rapidly changing irradiance. This loss in MPP tracking is because these algorithms do not have the inherent capability to differentiate between the change in power due to intentional perturbation or due to change in irradiance. Several authors have investigated this 'drift' phenomena and suggested modifications in HC algorithms to improve their tracking capability [5].

In [21], the authors proposed a voltage reference-based drift-free P&O algorithm, which tracks the MPP under rapidly changing irradiance. The algorithm uses an objective function evaluated by taking the slope of power vs duty curve to determine a change in irradiance. However, the algorithm has poor transient response under a sudden change in irradiance. The authors in [22] proposed a modified incremental resistance-based algorithm. Although, the algorithm uses a self-tuning IPID controller, the constant factor assumed depends on the PV power rating. In [23], the authors proposed a drift-free P&O boost converter based MPPT controller. The algorithm compares the sign of change in power, current and voltage to detect a change in irradiance. However, the algorithm loses its tracking capability if the point of operation shifts to the same side of the new curve. In [24], the algorithm compares the difference in power between two samples and compares the voltage of the last two samples to accurately detect a change in irradiance. However, the proposed algorithm offers a slow tracking speed. In [25], an adaptive incremental resistance method has been proposed that shifts the operating point to RHS of the I-V curve under sudden variations in irradiance and load resistance. Although, the algorithm promises a high tracking speed it can deviate from the MPP tracking path under continuously changing irradiance. In [26], the authors proposed a weighted set point similarity method in which four consecutive duty cycles are stored to determine the direction of tracking. The algorithm uses an upper and lower power boundary limits which are iteratively reduced to converge towards the MPP. If a sudden change in irradiance is observed, these limits are expanded and the whole process starts again. The performance of the algorithm is highly dependent on the constants used to determine the boundary limits. In [27], the authors proposed an improved incremental conductance in which the algorithm tracks the MPP by taking two step-sizes based on the region of operation. A small step-size is used under steady-state condition whereas a large step-size is taken under a change in irradiance or when the operating point is far away. The algorithms' performance is highly dependent on the chosen step-sizes and the constant value chosen for the steady-state region.

Apart from these, several authors have proposed MPPT algorithms based on evolutionary algorithms. In [28], recent developments have been reported in the ANN based tracking algorithms. Several other sophisticated MPPT techniques like genetic algorithm, particle swarm optimization, gravitational search algorithm, and other metaheuristic approaches have been proposed [29 – 33]. Although these techniques are efficient but require large memory and the use of an expensive hardware controller. Hence, hill-climbing algorithms remain the natural choice of selection for tracking the MPP.

In recent years, several researchers have compared and analyzed the performance of the conventional and adaptive hill-climbing (AHC) algorithms [34 – 39]. In [34], the authors have simulated and analyzed the performance of the CHC and AHC algorithms. Among them, adaptive algorithms performed well as compared to their conventional counterparts under medium-high irradiance levels. However, the performance of these algorithms remains relatively obscure as it does not take into account the ADC resolution, which remains a crucial aspect in real-time implementation of the MPPT algorithms [35]. In [36], a comparison among P&O, INC, and derivative dP/dt use the EN50530 test procedure to state that derivative dP/dt has the highest efficiency under high regulating frequency. In [37], the authors compared beta, temperature, ripple correlation, conventional and modified P&O and INC algorithms under medium-high insolation levels. Among the tested algorithms, the beta method exhibits good transient response and low steady-state oscillations. In [38], a comparison between improved HC MPPT algorithms is carried out. The analysis shows that fuzzy based P&O algorithm outperforms the conventional ones when subjected to severe changes in irradiance. In [39], the researchers have investigated the performance of fractional open-circuit voltage, INC, P&O and temperature based MPPT algorithms in MATLAB/Simulink environment. The results indicate that fractional open-circuit voltage has a higher efficiency but requires a large number of sensors. A literature survey is conducted showing previous similar works as in Table 1.

Several articles have discussed the performance of CHC and AHC algorithms under medium-high irradiance levels. However, very few studies have examined the efficacy of these algorithms under low insolation levels. A typical day in Kuala Lumpur has low insolation levels, below 400 W/m^2 and sudden changes for nearly 40% of the useful 10-hour day [40]. Similar conditions exist during the big-rain season (June-September) in Ethiopian highlands and may also exist in other tropical regions of the world [41]. Moreover, the niche applications of emerging PV technologies also signify that optimizing the yield from PV arrays under low irradiance is essential [42]. Hence, a detailed analysis of the HC MPPT algorithms becomes essential by evaluating and optimizing their performance under low irradiance levels.

The key novelty features of the proposed work are:

i) An in-depth study is carried by evaluating two distinct duty, current and voltage perturbation step-sizes for the MPPT algorithms corresponding to minimum and optimum change in voltage and current due to perturbation that is sensed by the ADC for a wide range of irradiance values.

ii) A generalized expression is derived for calculating the optimum step-size for the duty-based hill-climbing algorithms by considering the worst condition to ensure the correct operation of the MPPT algorithm.

iii) The current and voltage control loops are meticulously designed with the help of small-signal analysis to ensure the stability and robustness of the controller.

iv) The performance evaluation of eight HC MPPT algorithms is carried out for suboptimal and optimum perturbation step-sizes using a small-scale experimental prototype and further statistical analysis is carried out on the obtained results.

Table 1 Literature Review of previous similar works

Ref	Year	Algorithms	Type of Review	Irradiance Level	Results
[34]	2014	P&O, CV, A-P&O, INC, fractional SC current	Simulation	High	Quantitative
[35]	2016	CV, P&O, INC, FLC, ANN, Modified P&O, PI-FLC	Simulation	Medium High	Quantitative
[36]	2011	P&O, INC, *dP/dt*	Experimental	Low Medium High	Quantitative
[37]	2013	Beta, P&O, temperature, Modified INC, Correlation	Experimental	Medium	Quantitative
[38]	2019	P&O, INC, Fuzzy-P&O, Fuzzy-INC	Simulation	Low Medium High	Quantitative
[39]	2016	Fractional OC voltage, P&O, INC, temperature, FLC, ANN	Simulation	Medium High	Quantitative
[40]	2013	OC voltage, fractional SC, P&O, ESC, INC, AI	Simulation	Medium High	Qualitative
[41]	2014	CV, P&O, A-P&O	Experimental	High	Quantitative
[42]	2015	P&O, ANN, FLC, PSO, A-P&O, BST, DCPA	Simulation	High	Qualitative
[43]	2015	P&O, PSO, SA	Simulation	High	Quantitative
[44]	2016	P&O, INC	Simulation	High	Qualitative

[45]	2017	HC, Soft computing	Theoretical	-	Qualitative
[46]	2018	P&O, INC, model-based	Experimental	Medium High	Quantitative
[47]	2019	ESC, SM-ESC, modified-ESC	Experimental	Medium High	Quantitative
[48]	2019	P&O, A-P&O, DF-P&O, INC	Experimental	Medium High	Quantitative
[49]	2020	I&T, CV, TG, fractional OC voltage, fractional SC current, P&O	Experimental	Medium High	Quantitative
[50]	2021	P&O, A-P&O, A-INC, CSAM, ASF-beta, GAF-VPF	Simulation	Medium High	Quantitative
[51]	2021	Fixed zone P&O, A-INC, P&O	Experimental	Low Medium High	Quantitative

The article is structured as follows. Section 2 gives a brief overview of the commonly used Hill Climbing MPPT Techniques. Section 3 describes the methodology to evaluate the perturbation step-sizes based on the resolution of the ADC and the stability aspects in designing the MPPT controller. In section 4, the small-scale experimental setup used to test various MPPT algorithms, is explained. Section 5 covers the experimental results and statistical analysis of the implemented algorithms under both sudden changes in irradiance and uniform irradiance. In section 6, a detailed discussion on the performance of the various MPPT algorithms is carried out. Finally, section 7 concludes the study and gives the salient findings of the proposed work.

2. **Hill-Climbing MPPT Algorithms**

Hill-Climbing MPPT algorithms are primarily used in medium-high power AC/DC PV applications. This section briefly discusses the most common conventional and adaptive hill-climbing algorithms.

2.1.Perturb and Observe Algorithm

In this algorithm, the duty of the converter is purposefully disturbed to observe the change in power. This disturbance decides the tracking direction.

The duty-based P&O algorithm is governed by (1).

$$D(k) = D(k-1) \pm \text{Step} \quad (1)$$

where, $D(k)$ is the duty at K^{th} iteration, $D(k-1)$ is the duty at $(K-1)^{th}$ iteration and Step is the duty perturbation step-size.

Careful selection of perturbation step-size, ΔD governs the efficacy of the C-P&O algorithm. A high tracking speed may be achieved by increasing the step-size but with a penalty of increased power fluctuations around MPP, which can result in instability. A small perturbation step-size does improve the steady-state response, but slows down the tracking speed, as shown in Fig. 3. A-P&O algorithm improves this trade-off between steady-state power oscillations and tracking speed.

The perturbation step of A-P&O in (2) uses a scaling parameter, M, and also gathers knowledge on the slope of the power curve. The scaling parameter helps in quickly reaching the MPP with low power oscillations around MPP. Maximum duty step-size and the corresponding difference in voltage and power determine the scaling factor, M as in (3) [18].

$$\text{Step} = \text{M}\,\frac{|P(k-1)-P(k-2)|}{|V(k-1)-V(k-2)|}$$

(2)

$$\text{M} = \frac{|dV_{\max}| \times \Delta D_{\max}}{|dP_{\max}|}$$

(3)

where, ΔD_{max} = maximum step-size in duty, dV_{max} = change in voltage corresponding to ΔD_{max} and dP_{max} = change in power corresponding to ΔD_{max}. The combined flowchart of C-P&O and A-P&O algorithms is shown in Fig. 4.

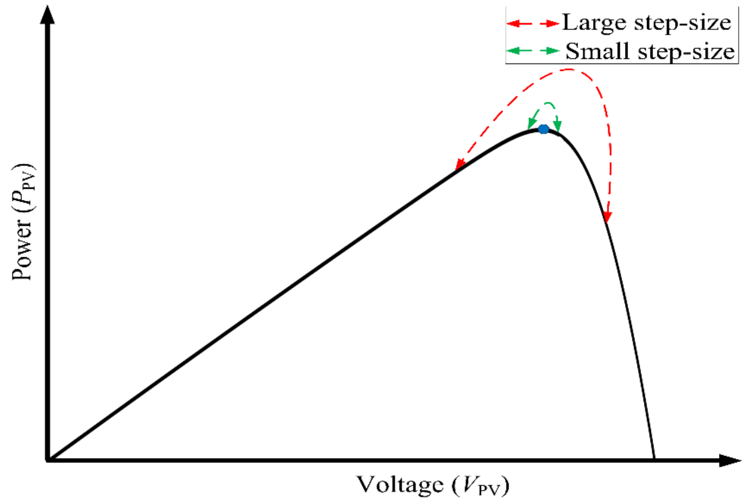

Fig. 3. Power oscillations around MPP under different step-sizes

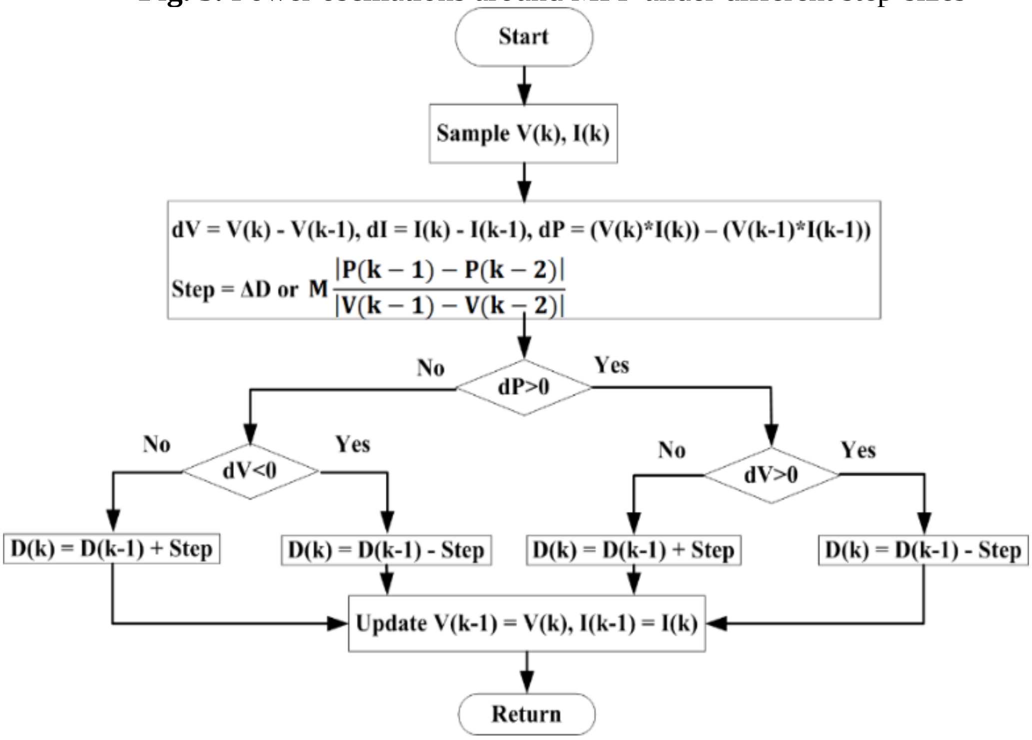

Fig. 4. Compiled Flowchart of Classical and Adaptive P&O MPPT algorithm

2.2.Incremental Conductance Algorithm

This algorithm is similar to the P&O algorithm [52]. It also uses the knowledge of the slope of the power curve, which decides the tracking direction. If the ratio of the increment in conductance is higher than the negative conductance, the reference voltage is increased to track MPP. If the ratio of the increment in conductance is less than the negative conductance, the reference voltage is decreased to track MPP. The combined flowchart of C-INC and A-INC algorithms is shown in Fig. 5.

The voltage-based INC algorithm is governed by (4):

$$V_{ref}(k) = V(k-1) \pm \text{Step} \quad (4)$$

The voltage step-size 'ΔV' governs the performance of the C-INC algorithm. A-INC algorithm uses a scaling parameter, N, and the knowledge of the power curve, which ensures a balance between maintaining low power oscillations and a high tracking process. The step-size of A-INC algorithm and the scaling parameter N is governed by (5) and (6), respectively [19].

$$\text{Step} = \text{N}\frac{|P(k-1)-P(k-2)|}{|V(k-1)-V(k-2)|} \tag{5}$$

$$\text{N} = \frac{|dV_{\max}|\times\Delta V_{\max}}{|dP_{\max}|} \tag{6}$$

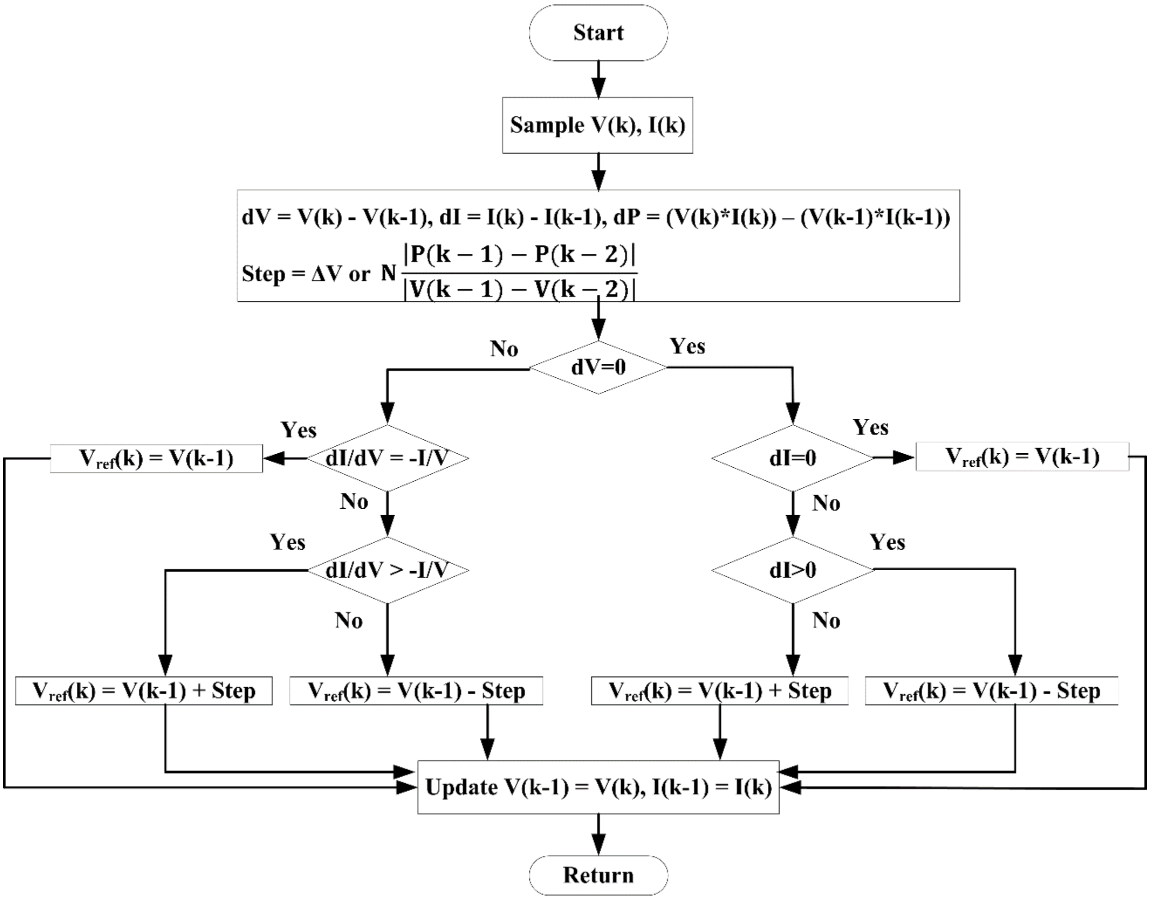

Fig. 5. Compiled Flowchart of C-INC and A-INC MPPT algorithm

where, $\Delta V_{\max}$ = maximum step-size in voltage, $dV_{\max}$ = ($\Delta V_{\max}$) maximum change in voltage corresponding to $\Delta V_{\max}$ and $dP_{\max}$ = maximum change in power corresponding to $\Delta V_{\max}$.

2.3.Incremental Resistance Algorithm

The INR algorithm also belongs to the family of the hill-climbing technique as it uses the information of the slope of the P-I power curve to track in the correct direction. The algorithm uses current as a perturbation parameter to track the MPP. If the ratio of change in output resistance is higher than the negative output resistance, the reference current is increased to track MPP. On the other hand, when the ratio of change in output resistance is less than the negative output resistance, the current reference is decreased to track MPP. The combined flowchart algorithm of C-INR and A-INR is in Fig. 6.

The INR algorithm is depicted by (7) as given below.

$$I_{\text{ref}}(k) = I(k-1) \pm \text{Step} \tag{7}$$

The perturbation step-size determines the performance of the classical INR algorithm in current, i.e., 'ΔI'. A significant value of ΔI improves the dynamic response on account of large steady-state oscillations, whereas a small value slows down the tracking process. The perturbation step-size of the adaptive INR algorithm in (8) tries to balance this trade-off with the help of a scaling parameter, C, and the knowledge of the P-I power curve [20].

$$\text{Step} = C\,\frac{|P(k-1)-P(k-2)|}{|I(k-1)-I(k-2)|} \tag{8}$$

The maximum step-size in current and the corresponding change in maximum power calculates the scaling factor, C, as in (9).

$$C = \frac{|dI_{\max}|\times\Delta I_{\max}}{|dP_{\max}|} \tag{9}$$

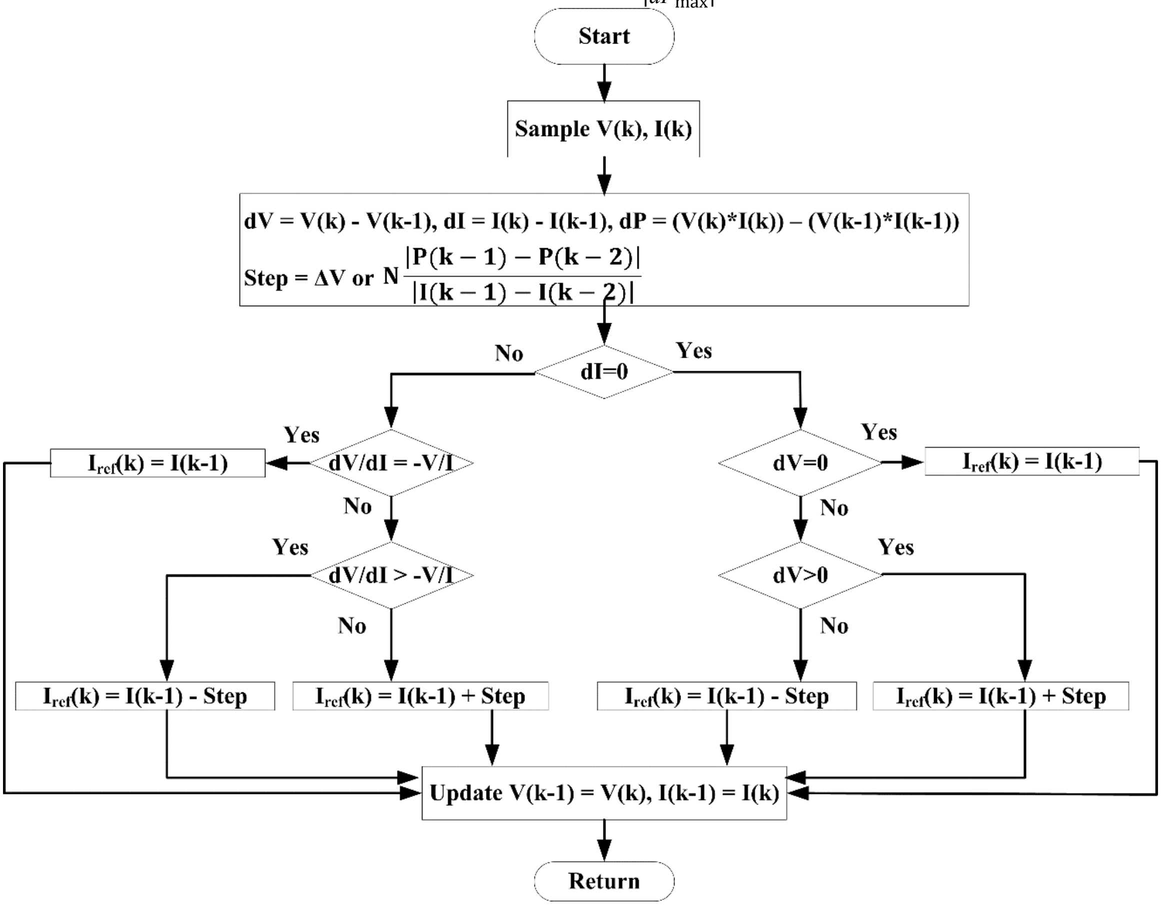

Fig. 6. Combined Flowchart of C-INR and A-INR algorithm

where, $\Delta I_{\max}$ = maximum step-size in current, $dI_{\max}$ = maximum change in current corresponding to $\Delta I_{\max}$, and $dP_{\max}$ = maximum change in power corresponding to $\Delta I_{\max}$.

It may not be out of place to mention here that direct-duty MPPT algorithms are not affected by the changes in the parameters of PV arrays due to aging [53]. Hence, the values of $\Delta V_{\max}$ in (6) and $\Delta I_{\max}$ in (9) may require periodic tuning to compensate for the aging effect.

2.4.Drift-Free Algorithm

In recent years, hill-climbing based drift-free MPPT algorithms have gained popularity due to their high accuracy in tracking the MPP under rapidly changing irradiance [34]. It is widely known that the conventional and adaptive hill-climbing MPPT algorithms suffer from drift-phenomena under rapidly changing irradiance. To elaborate on this concept, consider that the current operating point is at 1 in the low irradiance curve as shown in Fig. 7. Under constant irradiance, the conventional and adaptive HC MPPT algorithms operate normally and ensure that the point of operation will shift from 1 to 2 to extract more power. On the other hand, if there is a sudden change in irradiance while going from 1 to 2, the point of operation shifts from 1 to 3. This is due to the sudden increase in irradiance under constant load resistance. Now, the operating point 3 lies on the RHS of the high irradiance curve. The conventional and adaptive hill-climbing algorithms cannot determine the reason behind the increase in power, i.e. whether it is due to perturbation or due to an increase in irradiance. Hence, these algorithms allow perturbation in the same direction causing the point of operation to shift from 3 to 4, which results in power loss. This drift is severe in adaptive HC MPPT algorithms as these algorithms use large step-size corresponding to a large change in irradiance.

To overcome this, authors in [5], proposed a drift-free P&O MPPT algorithm that monitors an additional parameter, i.e. a change in current to determine whether the change in power is due to intentional perturbation or change in irradiance, as shown in Fig. 8. It can be easily observed that the sign of change in power, current and voltage between two perturbations is same only when there is a change in irradiance. This is due to the unique I-V characteristic of the PV module.

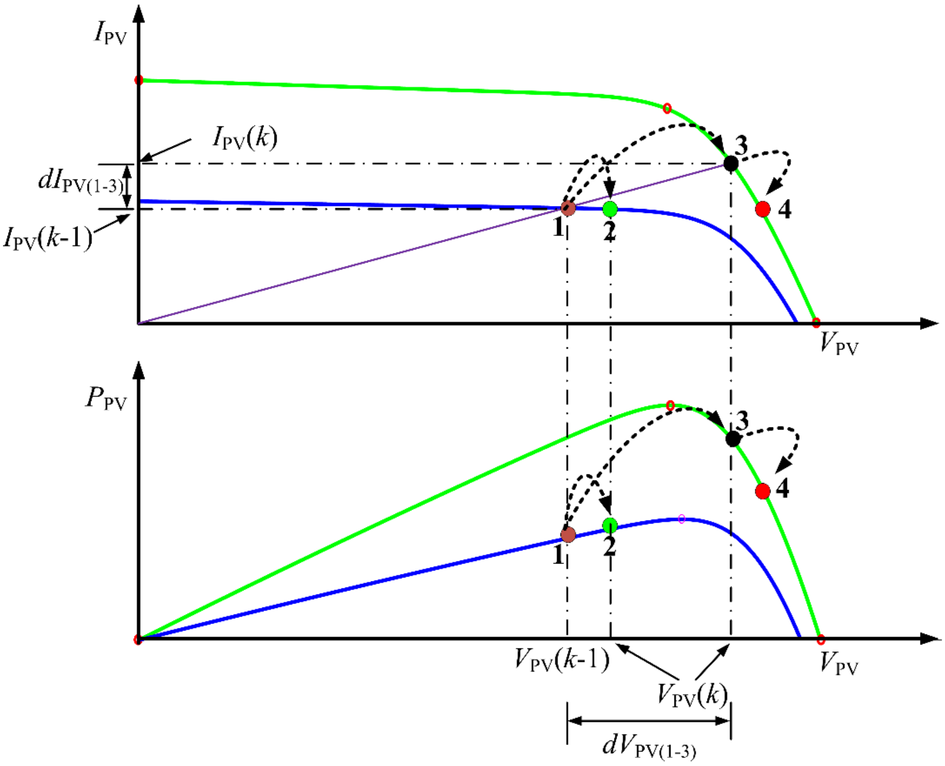

Fig. 7. Drift phenomena in hill-climbing MPPT algorithms

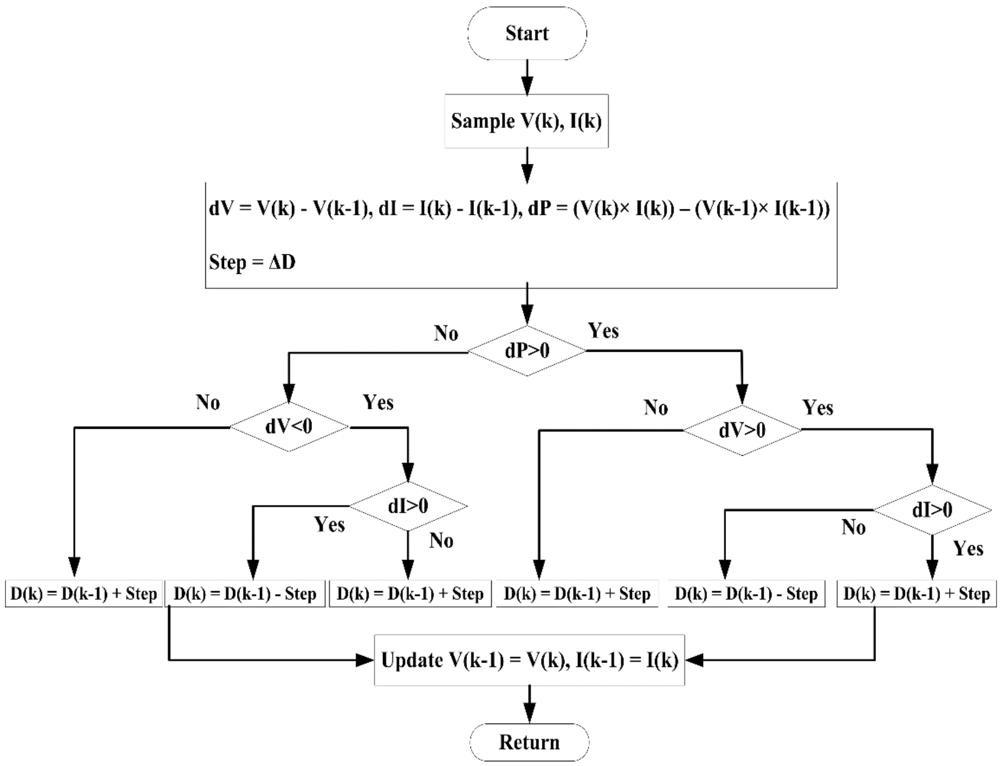

Fig. 8. Flowchart of conventional drift-free P&O algorithm

An adaptive drift-free MPPT algorithm is proposed in [54], which can overcome the drift under simultaneous changes in irradiance and load resistance. The algorithm detects the change in irradiance by comparing the sign of the slope of P-V and P-I curve between two perturbations, as shown in Fig. 9. The sign of the slope of the two power curves are same only when there is a change in irradiance. The algorithm uses two perturbation parameters, namely, voltage and current to ensure high speed of tracking and limits the oscillations around MPP by iteratively reducing the perturbation step-size.

This section has briefly overviewed the MPPT algorithms chosen for investigation under low irradiance condition. The next section will cover the design aspects to implement these algorithms in real-time to ensure overall stability of the system.

3. Perturbation Step-Size under Low Irradiance Levels

The perturbation parameter can be in the form of duty, voltage or current to implement MPPT algorithms. It is already proven that the mathematical comparison of the P&O and INC algorithm is similar in continuous time as well as in their discrete implementation [52]. Therefore, the implementation of the C-P&O and A-P&O algorithm uses duty as a perturbation parameter, whereas C-INC and A-INC algorithms use voltage as a perturbation parameter. The different perturbation parameters help to determine the efficacy of conventional and adaptive P&O and INC algorithms.

The classical and adaptive INR algorithms use current as a perturbation parameter as both these algorithms require the knowledge of the P-I curve to reach MPP. Detailed analysis of the perturbation step-sizes for P&O, INC and INR algorithms is in the subsequent section.

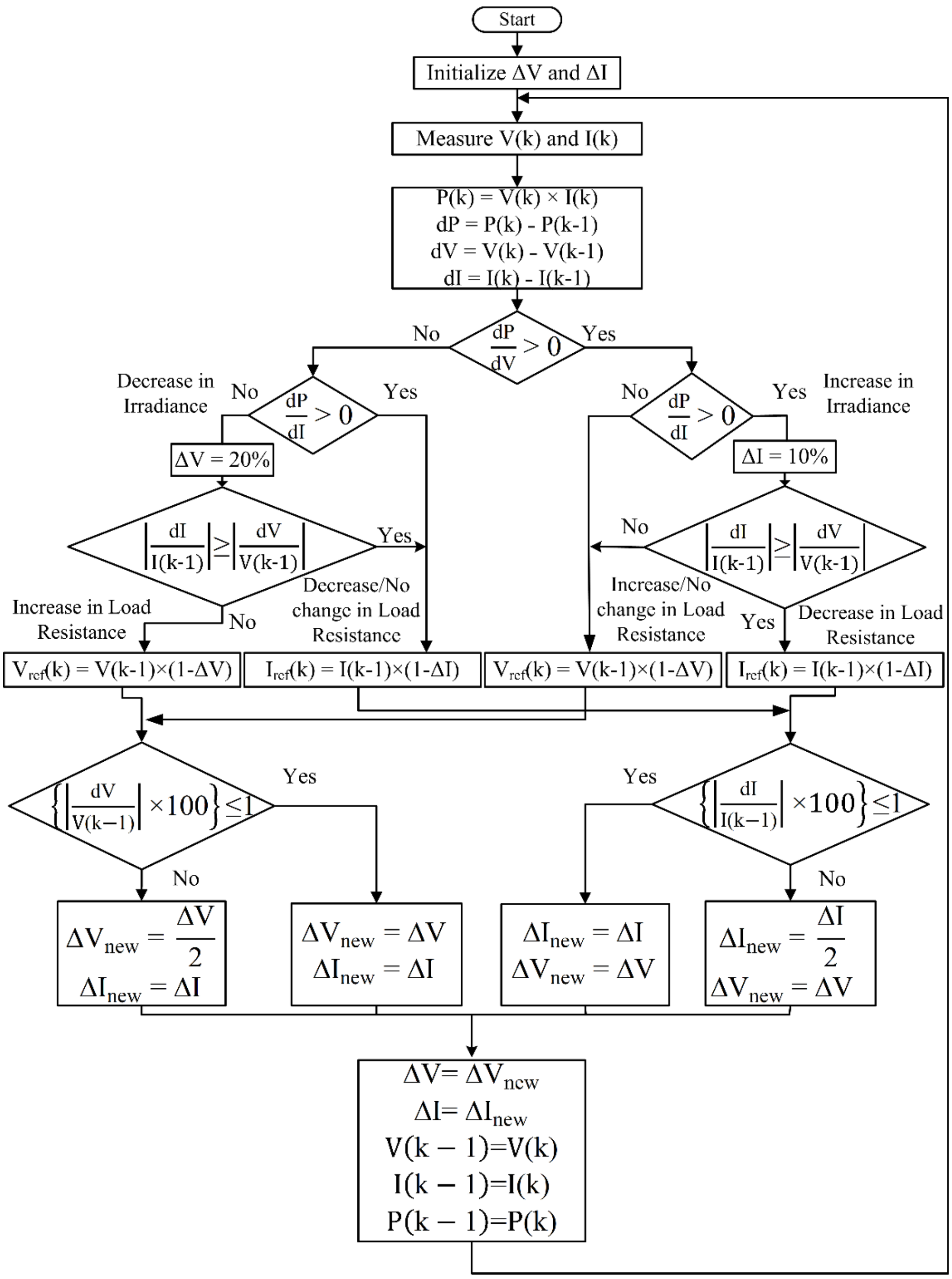

Fig. 9. Flowchart of adaptive drift-free MPPT algorithm

3.1.Calculation of Step-Size of C-P&O and A-P&O Algorithms

As mentioned previously, the P&O algorithm uses duty as the control variable. To accurately determine the perturbation step-sizes under low irradiance, the ADC resolution is a vital constraint variable. The experimental setup has an ADC of 10-bit resolution, with a maximum input voltage of 5V. Therefore, the minimum voltage that can be sensed by the ADC is 4.88mV. The current sensor has a sensitivity of 1mV/mA, the minimum sensing ability in voltage and current due to perturbation of the microcontroller is $dV_{\min}$ = 0.00488V and $dI_{\min}$ = 0.0488A, respectively. The perturbation step-sizes for different irradiance levels, for the minimum set values of $dV_{\min}$ and $dI_{\min}$, are given in Table 2.

From Table 2, one can easily observe that the perturbation step-size in duty is increasing as the irradiance decreases which is due to the set constraints on $dV_{\min}$ and $dI_{\min}$ values. A step-size of ΔD = 0.3922 is obtained under a low irradiance level of 250W/m^2 to detect a minimum change in voltage, $dV_{\min}$ = 0.00488V and current $dI_{\min}$ = 0.0488A. In C-P&O technique, step-size governs the yield of the algorithm. If a big step-size of 0.3922 is selected, then the performance of the algorithm may worsen under medium-high insolation level. On the other hand, a small step-size of 0.0087 under low irradiance conditions may give a false reading of ADC as the variation in voltage and current due to perturbation may fall below their minimum set values. This false reading of ADC will affect the operation of the MPPT algorithm. To determine an optimum perturbation step-size, the authors have changed the minimum difference in voltage and current value due to perturbation to be dV_{opt} = 0.1V and dI_{opt} = 0.01A, respectively. By doing this, the perturbation step-size is low, by marginally increasing the steady-state oscillations around MPP under high irradiance condition, as given in Table 3.

The designer should consider the resolution of the ADC for obtaining the optimum allowable change in voltage and current due to perturbation. Hence, the authors have determined generalized expressions for the optimum change in voltage and current as given in (10) and (11), respectively.

$$dV_{opt} = 2\times n\times dV_{min} \quad (10)$$

$$dI_{opt} = \frac{2\times n\times dI_{min}}{10} \quad (11)$$

where, n is the resolution of ADC and $dV_{min}(dI_{min})$ is the minimum value of voltage (current) that can be read by ADC.

Fig. 1 shows that the perturbation step change in voltage should be more than the perturbation step change in current to reach the MPP quickly [55]. The minimum perturbation step-size of ΔD = 0.0166 of 250W/m^2 is selected to ensure accurate tracking of both conventional and adaptive P&O algorithms.

The expression for optimum duty cycle at the lowest irradiance is derived an in (12), where, $D_{mpp(G)}$, $V_{mpp(G)}$ and I_{mpp}(G) is the duty cycle, voltage and current, respectively, at MPP at irradiance, G. Two values of ΔD_{opt} can be obtained from (12) corresponding to a minimum and maximum duty cycle. The maximum value of ΔD_{opt} should be selected for the worst condition and this value will ensure the correct operation of the P&O algorithm.

$$\Delta D_{opt}=\left|D_{mpp(G)}\text{-}D_{(max/min)}\right|=\sqrt{\frac{1}{R}}\left(\sqrt{\frac{V_{mpp(G)}\pm dV_{opt}}{I_{mpp(G)}\mp dI_{opt}}}-\sqrt{\frac{V_{mpp(G)}}{I_{mpp}(G)}}\right) \quad (12)$$

The value of scaling factor, M = 0.166 is obtained for dV_{max} = 0.3729V, D_{max} = 0.0166 and dP_{max} = 0.0371W by substituting these values in (3). These values are for the minimum irradiance level of 250W/m^2. The selection of these values ensures that the change in current and voltage due to perturbation never falls below the preset limit, under low irradiance (250W/m^2).

Table 2 Suboptimal duty perturbation step-sizes for dV_{min} = 0.00488V and dI_{min} = 0.0488A

***G* (W/m^2)**	1000	900	800	700	600	500	400	370	300	250
Δ*D*	0.0087	0.0110	0.0124	0.0157	0.0203	0.0296	0.0480	0.0643	0.1795	0.3922

3.2.Calculation of Step-Size of C-INC and A-INC Algorithms

As previously mentioned, the conventional and adaptive INC algorithms use voltage as a perturbation variable. Table 3 shows the step-sizes in voltage for different irradiance levels, with the same constraint on dV_{opt} and dI_{opt} values.

In this case, a minimum voltage step of ΔV = 0.3729V ensures accurate operation of the INC algorithms under all irradiance levels, as in Table 3. The direct increment/decrement in voltage is not possible as the control variable is duty cycle. The authors carefully designed a PI controller to implement the voltage based C-INC and A-INC algorithms.

3.2.1. Design of Voltage Control Loop

The MPPT controller circuit diagram for implementing P&O, INC, INR and DF MPPT algorithms is shown in Fig 10. The instantaneous value of voltage (V_{PV}) and duty (d) are perturbed to deduce the small-signal expression as given in (13) [56]:

$$G_{vd}(s)=\frac{\widetilde{V_{PV}}}{\tilde{d}}=\frac{\frac{V_o L s}{R}}{LCs^2+\frac{L}{R}s+(1\text{-}d)^2} \tag{13}$$

where, $\tilde{V}_{PV}$ and $\tilde{d}$ are small perturbations in PV voltage and duty, respectively.

The transfer function of the PI controller for the VCL is depicted by (14).

$$G_v(s)=K_{pv}+\frac{K_{iv}}{s} \tag{14}$$

The open-loop transfer function of the control loop is depicted by (15).

$$G_{olv}(s)=G_{vd}(s)G_v(s) \tag{15}$$

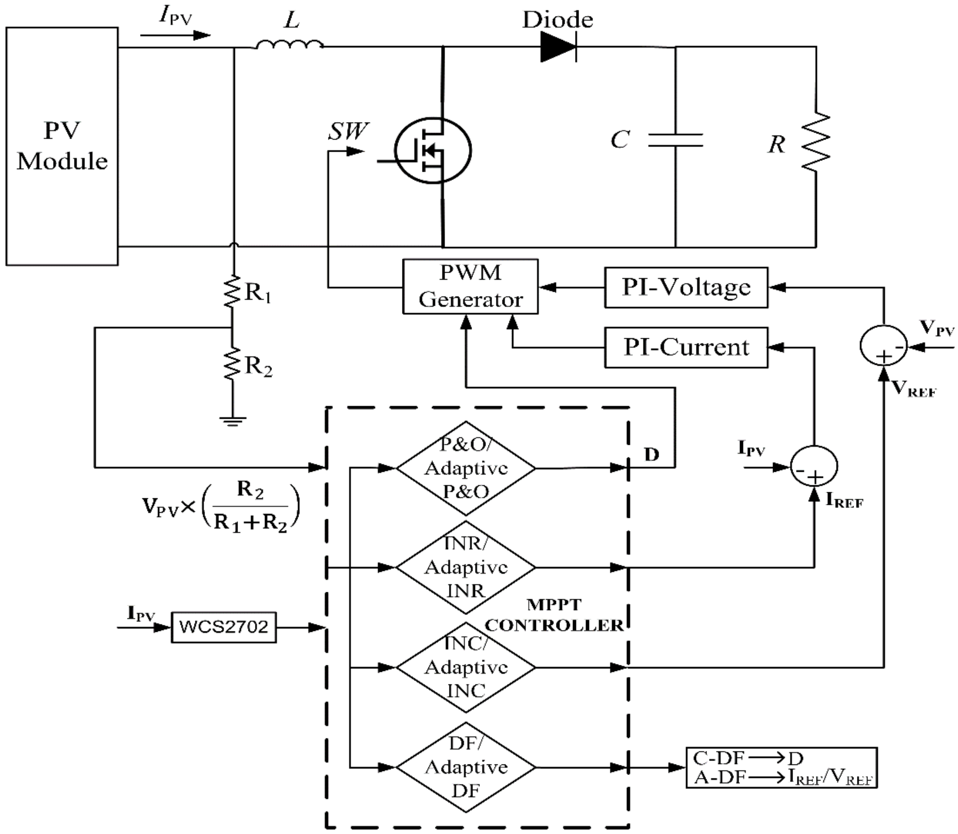

Fig. 10. Circuit diagram of the MPPT controller

Table 3 Optimum perturbation step-sizes for dV_{opt} = 0.1V and dI_{opt} = 0.01A

G (W/m²)	1000	900	800	700	600	500	400	370	300	250
Δ*D*	0.0024	0.0034	0.0034	0.0047	0.0068	0.0072	0.0084	0.0086	0.0149	0.0166
Δ*V* (V)	0.1000	0.1031	0.1034	0.1208	0.1410	0.1737	0.2190	0.2461	0.3100	0.3729
Δ*I* (A)	0.0200	0.0113	0.0112	0.0100	0.0100	0.0100	0.0100	0.0100	0.0100	0.0100

The bode graph of the control loop without and with compensation is shown in Fig. 11(a). The open-loop transfer function without compensator has a phase margin of -91.4° at 33.1 rad/s as shown in Fig. 11(a). The designed controller gives an overshoot of 5.8% for a unit step response having a phase margin (PM) of 60° at 8.95 krad/s. The coefficients calculated are K_{pv} = 0.348 and K_{iv} = 2059.8.

The root locus of the open-loop transfer function $G_{olv}(s)$ is shown in Fig. 11(b). The root locus shows that the closed-loop poles for 60° PM occur at $p_{1,2}$ = -266±j797 (ζ = 0.317, ω_n = 840 rad/s) which ensures the stability of the system.

The scaling factor, N = 3.661 obtained for dV_{max} = 0.3729V and dP_{max} = 0.03797W for adaptive INC algorithm using (6). These values are chosen for the minimum irradiance level of 250W/m² and will ensure the correct operation of the A-INC algorithm.

3.3. Calculation of Step-Size of C-INR and A-INR Algorithms

As the conventional and adaptive INR algorithms use the knowledge of the P-I curve, they use current as a perturbation variable. Table 3 shows the current perturbation step-sizes for different irradiance levels for dV_{opt} = 0.1V and dI_{opt} = 0.01A.

The current based INR algorithm uses a minimum current step-size of ΔI = 0.02A, such that both conventional and adaptive INR algorithms work accurately under a wide range of irradiance conditions. As direct perturbation in current is not possible, careful designing of PI controller is essential to implement the current based INR algorithm.

3.3.1. Design of Current Control Loop

The current controller determines the reference current (I_{ref}) using INR algorithm, as shown in Fig. 10. The instantaneous value of current (I_{PV}) and duty (d) are perturbed to deduce the small-signal expression as given in (16) [18]:

$$G_{\mathrm{id}}(\mathrm{s})=\frac{\widetilde{I_{\mathrm{PV}}}}{\tilde{\mathrm{d}}}=\frac{V_{\mathrm{o}}C\mathrm{s}+2\frac{V_{\mathrm{o}}}{\mathrm{R}}}{LC\mathrm{s}^2+\frac{L}{R}\mathrm{s}+(1\text{-d})^2}$$

(16)

where, $\widetilde{I_{\mathrm{PV}}}$ and $\tilde{\mathrm{d}}$ are small perturbations in PV current and duty, respectively.

The transfer function of the PI controller for the CCL is depicted by (17).

$$G_{\mathrm{c}}(\mathrm{s})=K_{\mathrm{pc}}+\frac{K_{\mathrm{ic}}}{\mathrm{s}} \tag{17}$$

The open-loop transfer function of CCL is depicted by (18).

$$G_{\mathrm{olc}}(\mathrm{s})=G_{\mathrm{id}}(\mathrm{s})G_{\mathrm{c}}(\mathrm{s}) \tag{18}$$

The bode plot of the CCL without and with compensation is shown in Fig. 12(a). The open-loop transfer function without compensation has a phase margin of 85.7^0 at 6.83 krad/s, as shown in Fig. 12(a). The step input response of the current control loop without compensation results in an overshoot of above 10%.

The designed PI controller achieves a maximum overshoot of 7.8% for a PM of 60^0 at 1.88 krad/s. The coefficients of this PI controller are K_{pc} = 0.195 and K_{ic} = 133.8.

The root locus of the open-loop transfer function $G_{\mathrm{olc}}(\mathrm{s})$ is shown in Fig. 12(b). Root locus shows that the closed-loop poles for 60° PM occur at p_1 = 0 and $p_{2,3}$ = -266±j797 (ζ = 0.317, ω_n = 840 rad/s) thereby ensuring the stability of the system.

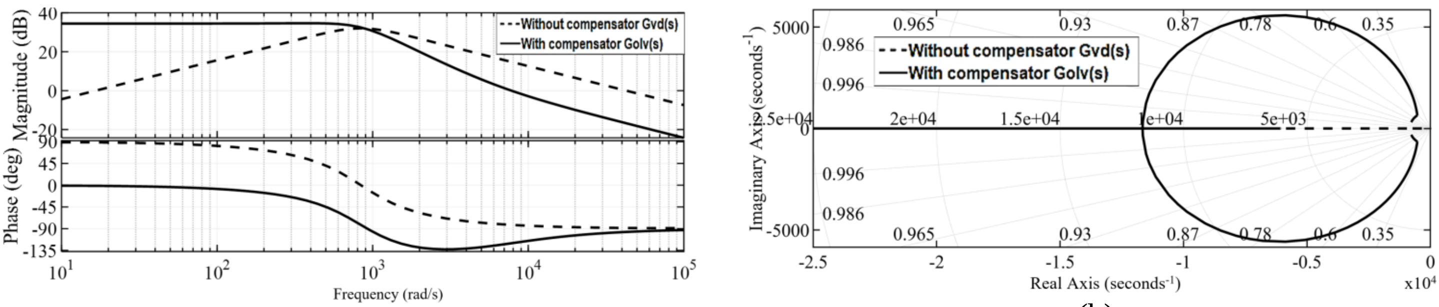

(a) (b)

Fig. 11. (a) Bode graph and (b) Root locus of VCL

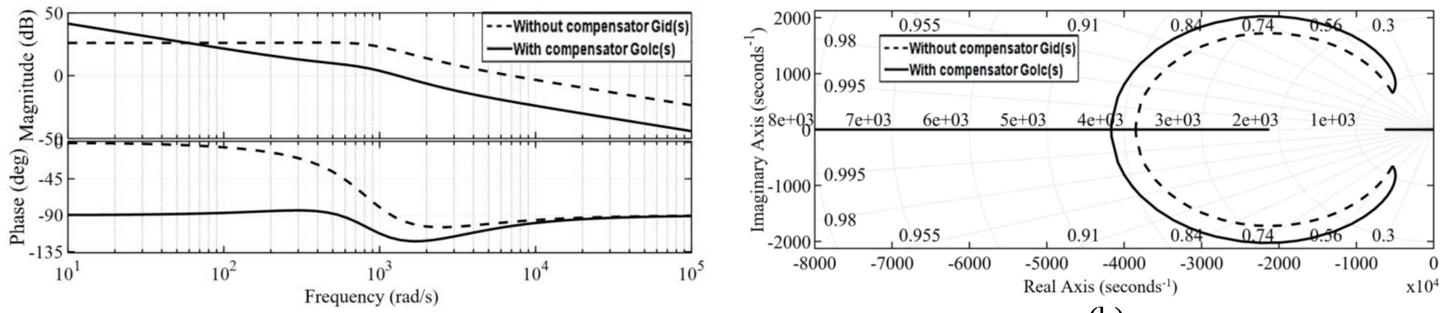

(a) (b)

Fig. 12. (a) Bode graph and (b) Root locus of CCL

The scaling factor, C = 2.9×10^{-3} is obtained for dI_{max} = 0.02A and dP_{max} = 0.1338W for adaptive INR algorithm using (9). The chosen value corresponding to the maximum irradiance level of 1000W/m^2 will ensure the reliable working of the adaptive INR algorithm under a wide range of irradiance.

4. Experimental Setup

A small-scale experimental setup developed to evaluate the performance of HC algorithms is shown in Fig. 13. For testing these algorithms, irradiance is varied over the Vikram Solar 40W (ELDORA 40P) multi-crystalline PV module by 150W halogen lamps whereas the module temperature is controlled through fans installed at the bottom of the PV module. The parameters of the 40W PV module are given in Table 4. MPPT algorithms are programmed in an inexpensive ATMEGA-32 microcontroller development board having ADC of 10-bit resolution. The voltage is sensed with the help of a potential divider circuit with R_1 = 10kΩ and R_2 = 1kΩ, whereas the current is sensed with the help of a current sensor (WSC2702) to reduce the maximum voltage given to ADC which should be less than 5V. Table 5 gives the specifications of the DC-DC boost converter which is designed for the MPP voltage and current values of the PV module at STC to ensure its stable operation under low and high irradiance levels. The boost converter control switch is a MOSFET (IRFP350) of 350V, 15A with low switching loss. A dedicated driver IC (IR2112) is used to drive the control switch. A constant load resistance, R = 60Ω is used to test the performance of the MPPT algorithms as shown in the circuit diagram of the MPPT controller in Fig. 10. Fluke 287 multi-meters and TDS2000C digital storage oscilloscope are used to store the experimental data.

5. Experimental Results

In this section, the authors analyzed the performance of the classical and adaptive algorithms for two distinct step-sizes under (i) sudden change in low values of irradiance and (ii) low values of uniform irradiance. The comparison between algorithms is carried out based on two key performance parameters as given below.

i) *Steady-state response time to reach MPP* (t_{ss}): The MPPT algorithms tracking speed is determined by the time taken by the algorithm to reach steady-state (t_{ss}) when there is a sudden change in the irradiance. In this study, the steady-state response time is evaluated by measuring the time taken by the algorithm to reach 90% of the target value.

ii) *Power oscillation around MPP*: The power oscillation is another key parameter to determine the performance of MPPT algorithms. It is calculated by taking the mean of samples of the difference between the target and the measured values. The power oscillations around MPP indicates the power loss, which is determined after the algorithm has reached steady-state.

Table 4 Specifications of 40W PV module at STC

N_C	V_{OC}	I_{SC}	V_{MPP}	I_{MPP}	β_{OC}	α_{SC}
36	21.95V	2.44A	17.84V	2.25A	-0.31V/^{0}C	0.058A/^{0}C

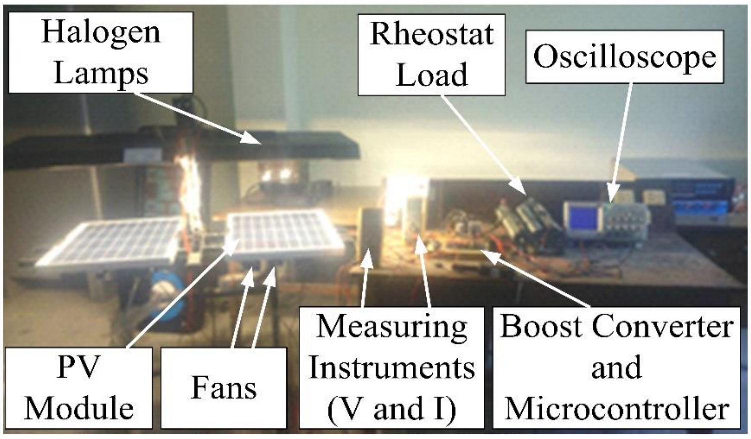

Fig. 13. Small-scale prototype to test the MPPT algorithms

Table 5 Parameters of the boost converter

V_{in}	I_{in}	V_{out}	D	R	L	C	f_{sw}
17.84V	2.25A	40V	0.554	40Ω	6mH	47μF	16kHz

5.1. Conventional vs adaptive P&O, INC, INR and DF algorithms for two distinct step-sizes under sudden variation in irradiance

In this case, the algorithms are tested on a 40W PV module under relatively constant temperature measured between T = 25°C – 25.5 °C. At t_1 = 0s, the MPPT algorithms are activated in succession with a starting irradiance of G = 250 W/m^2. At t_2 = 20s, the irradiance is instantly incremented to 370 W/m^2 and then instantly dropped to 250 W/m^2 at t_3 = 40s, as depicted by Fig. 14. The experimental waveforms of the MPPT algorithms for the suboptimal step-sizes corresponding to minimum ADC resolution are shown in Fig. 15.

Considering the ADC resolution, the minimum allowable change in voltage and current due to perturbation is dV_{min} = 0.00488V and dI_{min} = 0.0488A, respectively. The perturbation step of P&O, INC and INR algorithms corresponding to this condition are ΔD = 0.3922, ΔV = 0.8V and ΔI = 0.07A. As DF algorithm is implemented using duty as the perturbation parameter, ΔD = 0.3922 is used as the step-size. The Adaptive DF algorithm uses ΔV = 0.8V and ΔI = 0.07A as perturbation step-sizes for voltage and current, respectively. The zoomed P-t curves during start-up at t_1 = 0s, sudden increment in irradiance at t_2 = 20s and sudden decrement in irradiance at t_3 = 40s are shown in Fig. 15.

The observed response times of the MPPT algorithms with suboptimal step-size to reach steady-state around MPP are depicted in Table 6. Both conventional and adaptive P&O$_{SSS}$ and conventional DF$_{SSS}$ take more time to settle, as they fail to converge quickly due to the use of large step-size of ΔD = 0.3922. As the INC$_{SSS}$ algorithm uses voltage as a perturbation variable, the step-size of ΔV = 0.8V helps in quick convergence to MPP and hence, reaches steady-state at a faster rate. INR$_{SSS}$ algorithm comes out a close second with a low perturbation step-size of ΔI = 0.07A. The adaptive DF$_{SSS}$ is the fastest due to the two perturbation parameters used within the algorithm.

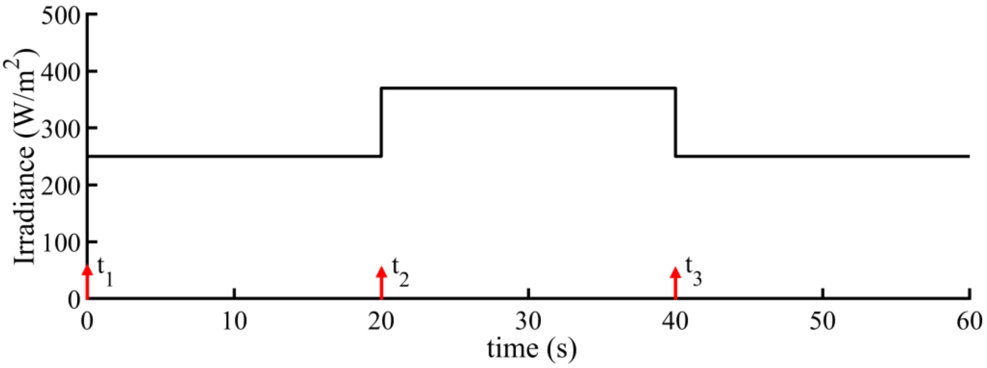

Fig. 14. Waveform indicating the change in irradiance

Although, a high step-size guarantees a rapid convergence, however, the use of a very large step-size of ΔD = 0.3922 and ΔI = 0.07A of P&O and INR algorithms, respectively results in instability and substantial power loss under steady-state power oscillations.

From Table 6, one can easily see that the SSS corresponding to the resolution of ADC, slightly improves the tracking speed. However, this also results in high power oscillations around MPP, which is due to the large step-size.

To maintain the balance between response time to reach SS and power oscillations around MPP, the authors have evaluated step-sizes using (10), (11) and (12). The expressions in (10) and (11) can guide an engineer to calculate the minimum allowable change in voltage and current, respectively, due to perturbation. Once the minimum step change in voltage and current is defined, one can obtain the optimum step-size using (12). The optimum allowable change in voltage and current due to perturbation is determined as dV_{opt} = 0.1V and dI_{opt} = 0.01A, respectively. The duty step-size for P&O$_{OSS}$ and DF$_{OSS}$ corresponding to these limits is ΔD = 0.0166. The voltage and current step-size for INC$_{OSS}$ and INR$_{OSS}$ are ΔV = 0.3729V and ΔI = 0.02A by taking into account the entire range of irradiance. The voltage and current step-size selection for INC and INR algorithms are chosen for the lowest and highest irradiance values of

250W/m^2 and 1000W/m^2, respectively. If we select the voltage step-size of the largest value of irradiance and current step-size for the lowest value of irradiance, there is a good chance that the change in voltage or current due to perturbation may fall below their minimum preset values.

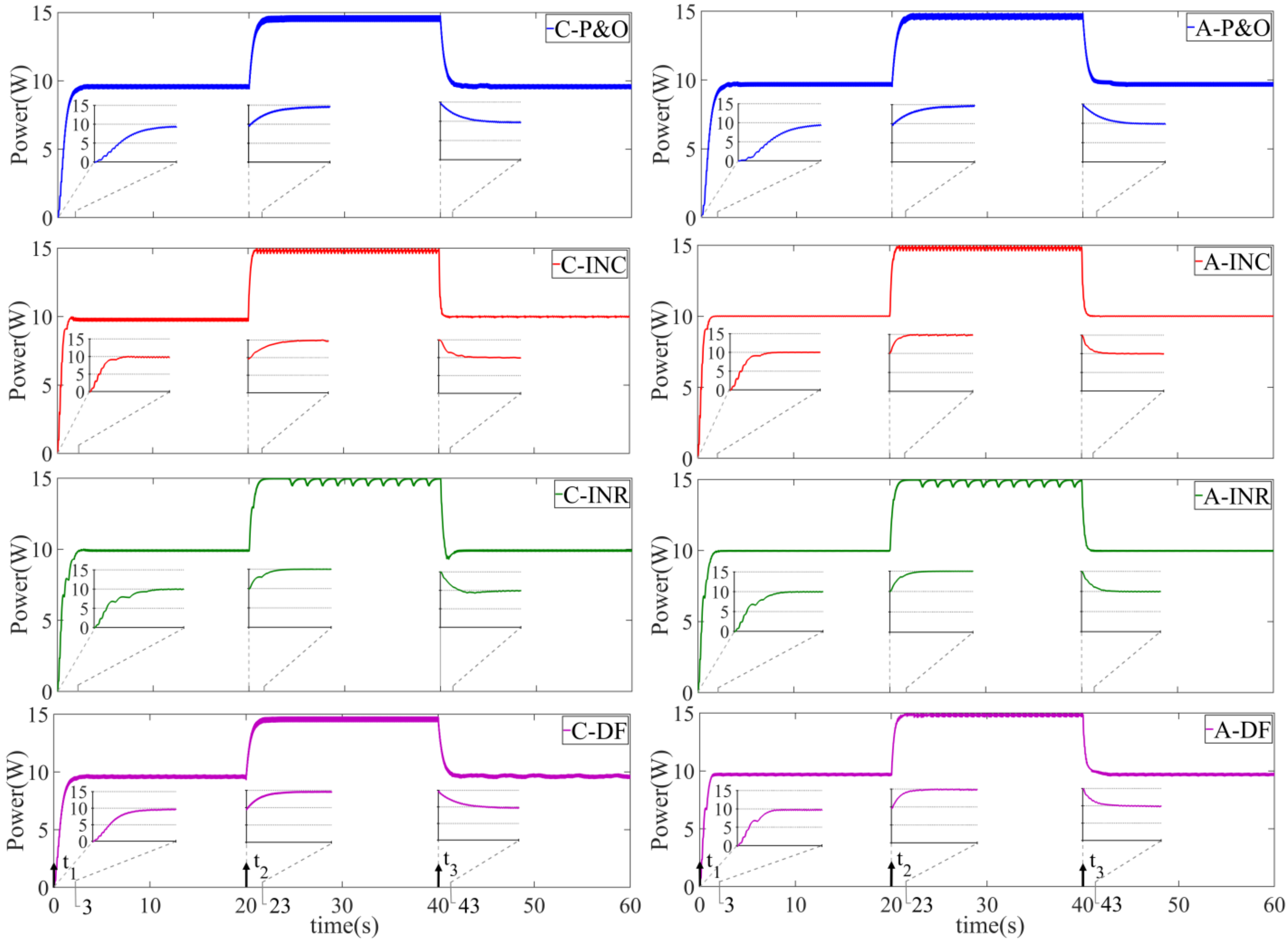

Fig. 15. Experimental waveforms of conventional and adaptive versions of P&O, INC, INR and DF MPPT algorithms under start-up at t_1 = 0s, increase in irradiance t_2 = 20s and decrease in irradiance at t_3 = 40s with suboptimal step-size (SSS), i.e., corresponding to ADC resolution

Table 6 Response time to reach steady-state (t_{ss}) of MPPT algorithms with SSS and OSS

Algorithm	t_{ss} during start-up (s)	t_{ss} under rising G (s)	t_{ss} under falling G (s)
P&O$_{SSS}$	2.1	1.4	1.1
INC$_{SSS}$	1.4	0.7	0.6
INR$_{SSS}$	2.5	0.8	1.4
DF$_{SSS}$	1.6	0.7	0.7
Adaptive P&O$_{SSS}$	2.1	1.4	1.1
Adaptive INC$_{SSS}$	1.4	0.7	0.6
Adaptive INR$_{SSS}$	1.7	0.7	0.5
Adaptive DF$_{SSS}$	1.4	0.6	0.5
P&O$_{OSS}$	2.1	1.7	0.8
INC$_{OSS}$	2.8	1.0	1.2

INR_{OSS}	2.2	0.8	1.3
DF_{OSS}	2.1	0.9	0.6
Adaptive $P\&O_{OSS}$	1.2	0.8	0.6
Adaptive INC_{OSS}	1.4	1.0	0.7
Adaptive INR_{OSS}	2.0	0.9	0.9
Adaptive DF_{OSS}	**1.4**	**0.7**	**0.5**

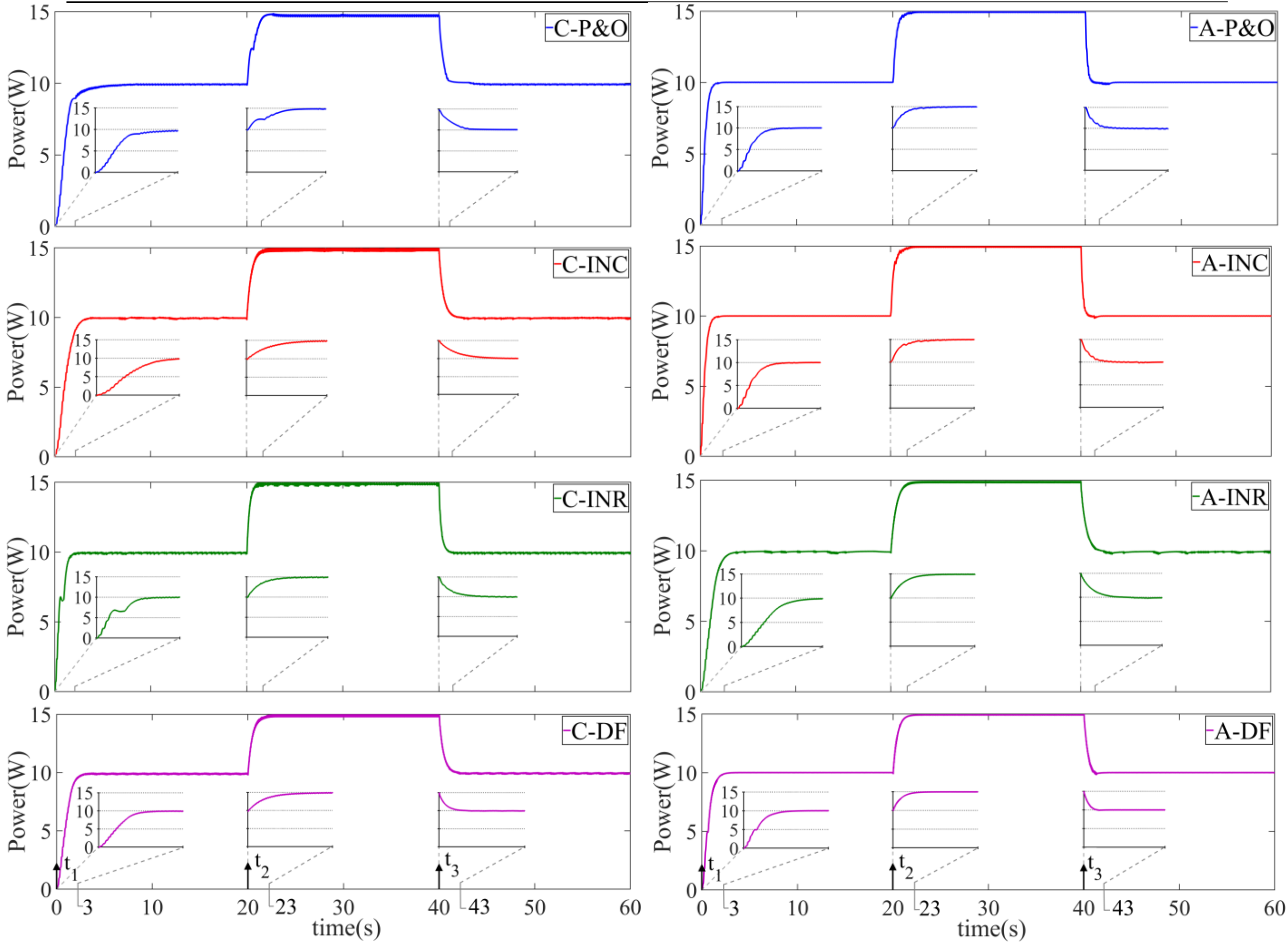

Fig. 16. Experimental waveforms of conventional and adaptive versions of P&O, INC, INR and DF MPPT algorithms under start-up at t_1 = 0s, increase in irradiance t_2 = 20s and decrease in irradiance at t_3 = 40s with optimum step-size (OSS)

The adaptive DF_{OSS} uses a voltage and current step-size of ΔV = 0.3729V and ΔI = 0.02A, respectively. The experimental waveforms of conventional $P\&O_{OSS}$, INC_{OSS} and INR_{OSS} algorithms with their adaptive versions for ΔD = 0.0166, ΔV = 0.3729V and ΔI = 0.02A under sudden change in irradiance are shown in Fig. 16. The zoomed experimental waveforms depicting the P-t curves under start-up at t_1 = 0s, increase in irradiance at t_2 = 20s and decrease in irradiance at t_3 = 40s are shown in Fig. 16.

Response times of the MPPT algorithms with the OSS to reach steady-state around MPP are given in Table 6. The results show that adaptive DF_{OSS} has the highest tracking speed, owing to dual perturbation, which results in low response time to reach steady-state around MPP. Adaptive $P\&O_{OSS}$ also has a good tracking speed due to direct duty perturbation, whereas adaptive INC_{OSS}/INR_{OSS} comes at a close third place. As the perturbation step-size is selected for the worst possible condition, similar response times among the conventional hill-climbing algorithms is noticed, under low irradiance levels.

As previously discussed, the worst possible condition for P&O and INC occurs under low irradiance, whereas in INR algorithm, it occurs at the highest possible irradiance. By selecting the perturbation step-size for worst conditions, the successful operation of ADC and thereby the reliability of the MPPT algorithm is increased for a broad span of irradiance. Under low irradiance, the change in voltage and current is small; therefore, the resolution of ADC becomes an important constraint in tracking the MPP.

5.2. Conventional vs adaptive P&O, INC, INR and DF algorithms for two distinct step-sizes under uniform irradiance condition

In the second case, the conventional MPPT algorithms are tested for two distinct step-sizes under low value of uniform irradiance levels, namely, 250 W/m^2 and 370 W/m^2. This case study helped in determining the power oscillations around MPP. The experimental results are analyzed, and a comparison based on steady-state power oscillations between the conventional and adaptive MPPT algorithms for two distinct step-sizes is shown in Table 7.

From the obtained results, one can see that the SSS corresponding to the ADC resolution, i.e., P&O$_{SSS}$, INC$_{SSS}$, INR$_{SSS}$ and DF$_{SSS}$ results in high steady-state oscillations. The power oscillations will keep on increasing as we go towards the higher value of irradiance. The OSS of the conventional MPPT algorithms results in low steady-state power oscillations because the change in voltage and current due these step-sizes is much greater than the resolution of ADC.

Hence, the perturbation step-size should be selected based on the worst possible condition such that the difference in voltage and current is always higher than the minimum set values, which can be easily read by ADC. These worst conditions occur in the case of conventional and adaptive INR algorithms at high irradiance levels. On the other hand, such worst conditions occur at low irradiance levels for the conventional and adaptive P&O and INC algorithms, thereby establishing that performance analysis in the medium-low range of irradiance cannot be ignored.

5.3. Robustness and Statistical Analysis

This section compares the performance of the MPPT algorithms by evaluating the mean, minimum, maximum and standard deviation of the extracted power using the statistical analysis. The mean is calculated to determine the accuracy of the different MPPT algorithms, whereas the standard deviation helped in measuring the amount of dispersion within the power data sets. Two non-parametric tests are performed to evaluate the overall performance of each MPPT algorithm.

To check whether Adaptive DF$_{OSS}$ outperforms other HC algorithms, Wilcoxon rank-sum test is performed with a significance level of $\alpha = 0.05$. The sign '+' indicates that the Adaptive DF$_{OSS}$ performs significantly better than the other algorithm, the sign '$\approx$' indicates that the Adaptive DF$_{OSS}$ is comparable to other algorithm and the sign '$-$' indicates that the Adaptive DF$_{OSS}$ algorithm is worse than the other algorithm. Table 8 gives the statistical results obtained by testing all eight algorithms under 370 W/m^2 and 250 W/m^2 irradiance.

Another non-parametric Friedman ranking test is performed to determine the ranking of the HC MPPT algorithms. Table 9 gives the ranking obtained using the Friedman ranking test which also shows that the Adaptive DF$_{OSS}$ algorithm has a superior tracking performance as compared to other algorithms.

Table 7 MPPT algorithms steady-state power oscillations for two distinct step-sizes

Algorithm	Power Oscillation (%) at 370 W/m^2	Power Oscillation (%) at 250 W/m^2
P&O$_{SSS}$	3.33	3.28
INC$_{SSS}$	3.20	3.18
INR$_{SSS}$	3.26	3.08
DF$_{SSS}$	3.18	3.17
Adaptive P&O$_{SSS}$	2.72	2.65
Adaptive INC$_{SSS}$	2.73	2.62
Adaptive INR$_{SSS}$	2.99	3.01
Adaptive DF$_{SSS}$	2.66	2.54

P&O$_{OSS}$	1.73	2.18
INC$_{OSS}$	1.66	2.08
INR$_{OSS}$	1.46	1.99
DF$_{OSS}$	1.64	1.98
Adaptive P&O$_{OSS}$	1.72	2.15
Adaptive INC$_{OSS}$	1.64	1.88
Adaptive INR$_{OSS}$	1.42	1.75
Adaptive DF$_{OSS}$	**1.38**	**1.35**

The distribution of extracted power obtained from the various HC algorithms is shown in the form of boxplot in Fig. 17. This distribution clearly shows the convergence accuracy and the sustained power oscillations in each MPPT algorithm.

From the statistical analysis it can be easily seen that the adaptive versions perform better than their conventional counterparts when implemented using OSS. The use of OSS also prevents false tracking process within the MPPT algorithm as the ADC resolution is not challenged.

Table 8 Statistical results using Wilcoxon rank-sum test with OSS

Irradiance	Algorithm	Power (W)				
		Max	Min	Mean	Std	rank-sum
250 W/m^2	**A-DF$_{OSS}$**	**10.03**	**9.91**	**9.96**	**0.03**	
	P&O$_{OSS}$	9.75	9.38	9.60	0.10	(+)
	INC$_{OSS}$	9.89	9.62	9.77	0.08	(+)
	INR$_{OSS}$	9.99	9.82	9.89	0.04	(+)
	DF$_{OSS}$	9.78	9.38	9.61	0.10	(+)
	A-P&O$_{OSS}$	9.84	9.51	9.71	0.09	(+)
	A-INC$_{OSS}$	9.84	9.51	9.71	0.09	(+)
	A-INR$_{OSS}$	9.84	9.52	9.70	0.07	(+)
370 W/m^2	**A-DF$_{OSS}$**	**15.01**	**14.41**	**14.84**	**0.14**	
	P&O$_{OSS}$	14.79	13.77	14.52	0.16	(+)
	INC$_{OSS}$	14.98	14.56	14.78	0.08	(+)
	INR$_{OSS}$	15.00	14.40	14.86	0.13	(≈)
	DF$_{OSS}$	14.79	13.79	14.53	0.16	(+)
	A-P&O$_{OSS}$	14.86	13.93	14.60	0.15	(+)
	A-INC$_{OSS}$	14.99	14.56	14.78	0.08	(+)
	A-INR$_{OSS}$	15.01	14.41	14.84	0.14	(≈)

Table 9 Ranking of the HC MPPT algorithms according to Friedman ranking test

Algorithm	Friedman ranking at 250 W/m^2	Friedman ranking at 370 W/m^2	Overall ranking
P&O$_{OSS}$	7.85	7.01	8
INC$_{OSS}$	5.81	4.98	5
INR$_{OSS}$	2.40	2.23	2
DF$_{OSS}$	7.00	6.36	7
A-P&O$_{OSS}$	5.01	5.56	6
A-INC$_{OSS}$	4.16	5.04	4
A-INR$_{OSS}$	3.72	3.01	3
A-DF$_{OSS}$	**1.82**	**1.99**	**1**

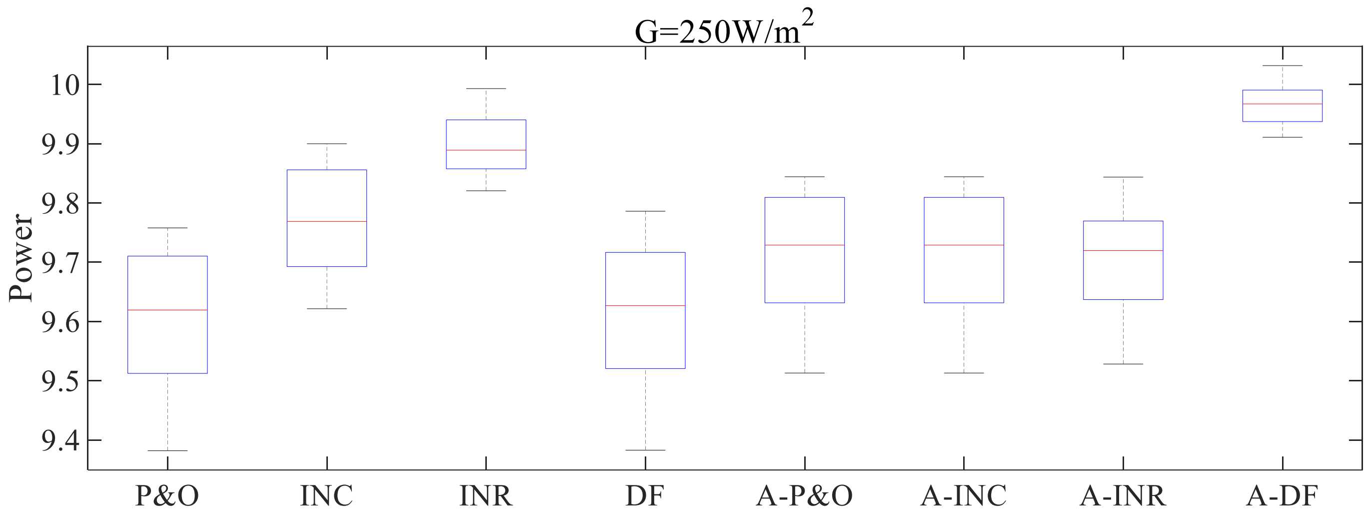

(a)

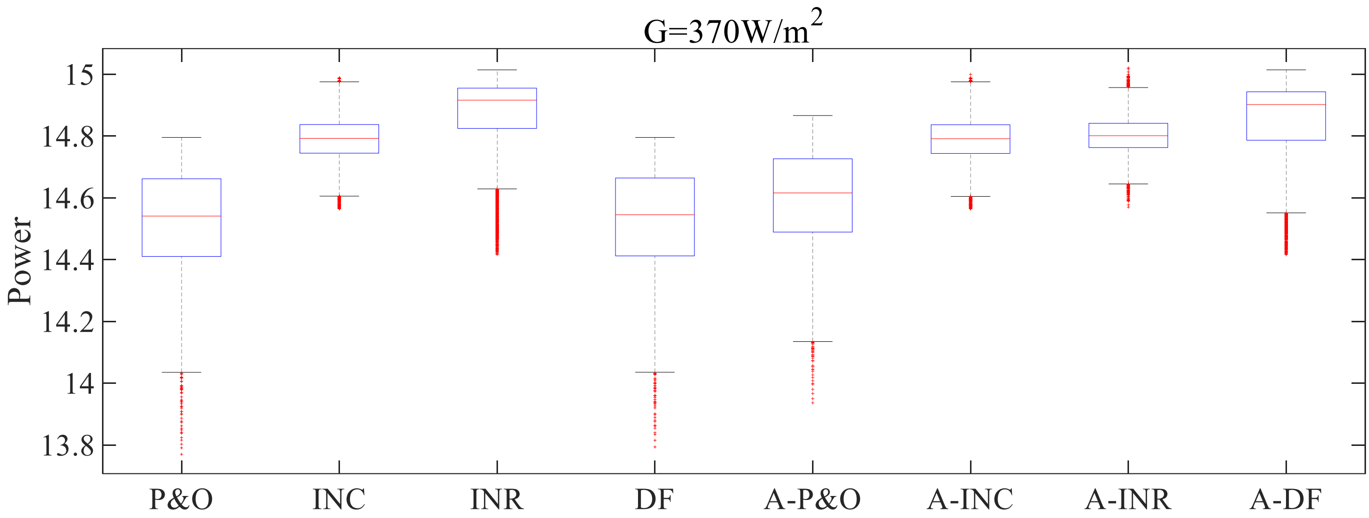

(b)

Fig. 17 Boxplot graph delineating the extracted Power (W) under (a) 250 W/m^2 and (b) 370 W/m^2

6. Discussion

To evaluate the performance of MPPT algorithm under low irradiance conditions, eight well established HC algorithms have been thoroughly investigated. It is observed that the perturbation step-size is a key parameter that governs the performance of the MPPT algorithm and should be carefully evaluated by considering the ADC resolution of the controller. The algorithm's performance is determined by evaluating the steady-state response time and the power oscillations around MPP at steady-state.

Under 250 W/m^2 and 370 W/m^2, the Adaptive DF algorithm has the lowest steady-state response time implemented for both SSS and OSS as compared to other HC algorithms. This is due to the use of two perturbation parameters, i.e. both voltage and current which increases the speed of tracking. The other adaptive algorithms when tested using SSS has a large settling time due to the large step-size which is calculated by considering the resolution of the ADC. Both conventional and adaptive versions of P&O, INC and INR algorithms show similar response time when implemented using SSS. To improve the tracking process the OSS remain the obvious choice under low irradiance conditions as they significantly improve the tracking speed of both conventional and adaptive HC algorithms.

The Wilcoxon rank-sum test is used to evaluate the standard deviation which helped in determining the dispersion in steady-state power. The test is used to compare the performance of the HC MPPT algorithms. The boxplot graphs under 370 W/m^2 indicate that the Adaptive DF and INR algorithms have similar dispersion in steady-state power. This is because of the low perturbation step-size in current determined by considering the optimum change in voltage and current due to perturbation that is sensed by the ADC. However, under 250 W/m2 the Adaptive DF algorithm outperforms the other HC algorithms as evident from the lowest standard deviation value obtained from the Wilcoxon rank-sum test.

Finally, Friedman ranking test is used to determine the overall rank of the various HC algorithms. The Adaptive DF algorithm remains the obvious choice even under low irradiance. The Conventional and Adaptive INR algorithms comes at a close second and third place due to the low perturbation step-size which although slightly increases the tracking time but has low steady-state power oscillations. Both Conventional and Adaptive P&O has a very good tracking speed but results in higher power oscillations at steady-state. The Conventional and Adaptive INC algorithm has similar tracking performance as compared to INR algorithms and has low steady-state oscillations when compared with P&O algorithms.

Hence, the proposed methodology to evaluate the optimum step-size is vital to improve the tracking response as well as ensure low steady-state oscillations around MPP especially under low irradiance.

7. Conclusion

This paper has compared and analyzed CHC and AHC algorithms for two distinct step-sizes under low irradiance levels. The imposition on the two preset values for the minimum allowable difference in voltage and current helped in comparing the performance of these algorithms. The first preset value is selected solely based on the resolution of the ADC. The authors proposed the second optimum preset value, such that the minimum allowable difference in current and voltage due to perturbation remains fairly larger than the resolution of the ADC. Two distinct step-sizes have been determined corresponding to these two preset values.

The selection of proposed preset value helped in reducing the perturbation step-sizes of conventional hill-climbing algorithms. The authors determined a method to evaluate the optimum duty step-size by taking the ADC resolution as a critical attribute to ensure the correct operation of the MPPT algorithm for the entire range of irradiance.

The major conclusions of the proposed work are as follows:

- The perturbation step-size should be evaluated based on the resolution of the ADC of the controller.
- The experimental results show that Adaptive DF algorithm is superior to other HC algorithms, in terms of tracking speed and low steady-state power oscillations.
- The small-signal modelling is vital to ensure the stability of both voltage and current control loop.
- The performance of the HC algorithms is similar when implemented using the SSS, because of the large perturbation step-size which is determined corresponding to the resolution of the ADC.
- Among P&O, INC and INR algorithms, the P&O algorithm has the highest tracking speed due to the use of duty as a perturbation parameter which helps in reducing the tracking time.
- The perturbation step-size should be optimized for the worst condition, i.e., analysis should be carried out for the lower end of irradiance.
- The proposed methodology to determine the OSS helped in lowering the steady-state oscillations and maintaining a good tracking speed.

This work will, hopefully, guide researchers, engineers and industry professionals working in this area to understand the key aspects when implementing MPPT algorithms and in evaluating their performance under low irradiance conditions. Furthermore, the performance of these MPPT algorithms can be analyzed on a grid-connected PV configuration for practical applications.

Acknowledgement

This work is supported in part by the European Commission H2020 TWINNING JUMP2Excel (Joint Universal activities for Mediterranean PV integration Excellence) project under grant 810809.

References

[1] EIA - Annual Energy Outlook 2019. https://www.eia.gov/outlooks/aeo/.
[2] Philibert C, 2011. Solar Energy Perspectives. International Energy Agency.
[3] McEvoy A, Markvart T, Castañer L, 2012. Practical Handbook of Photovoltaics: Fundamentals and Applications. Elsevier.
[4] Joshi P, Arora S. Maximum power point tracking methodologies for solar PV systems – A review. Renew Sustain Energy Rev 2017;70:1154–1177.
[5] Killi M, Samanta S, Modified Perturb and Observe MPPT Algorithm for Drift Avoidance in Photovoltaic Systems. IEEE Trans Ind Electron 2015;62:5549–5559.
[6] Subudhi B, Pradhan R. A Comparative Study on Maximum Power Point Tracking Techniques for Photovoltaic Power Systems. IEEE Trans Sustain Energy 2013;4:89–98.
[7] Li X, Wang Q, Wen H, Xiao W. Comprehensive Studies on Operational Principles for Maximum Power Point Tracking in Photovoltaic Systems. IEEE Access 2019;7:121407–121420.
[8] Kumer Podder A, Kumar Roy N, Roy Potta H. MPPT methods for solar PV systems: a critical review based on tracking nature. IET Renew Power Gener 2019;13:1615–1632.
[9] Karami N, Moubayed N, Outbib R. General review and classification of different MPPT Techniques. Renew Sustain Energy Rev 2017;68:1–18.
[10] Verma D, Nema S, Shandilya AM, Dash SK. Maximum power point tracking (MPPT) techniques: Recapitulation in solar photovoltaic systems 2016;54:1018–1034.
[11] Bendib B, Belmili H, Krim F. A survey of the most used MPPT methods: Conventional and advanced algorithms applied for photovoltaic systems. Renew Sustain Energy Rev 2015;45:637–648.
[12] Eltawil MA, Zhao Z. MPPT techniques for photovoltaic applications. Renew Sustain Energy Rev 2013;25:793–813.
[13] Sumathi V, Jayapragash R, Bakshi A, Akella PK. Solar tracking methods to maximize PV system output – A review of the methods adopted in recent decade. Renew Sustain Energy Rev 2017;74:130–138.
[14] Issaadi W, Issaadi S, Khireddine A. Comparative study of photovoltaic system optimization techniques: Contribution to the improvement and development of new approaches. Renew Sustain Energy Rev 2018;82:2112–2127.
[15] Ram JP, Babu TS, Rajasekar N. A comprehensive review on solar PV maximum power point tracking techniques. Renew Sustain Energy Rev 2017;67:826–847.
[16] Danandeh MA, Mousavi SM. Comparative and comprehensive review of maximum power point tracking methods for PV cells. Renew Sustain Energy Rev 2018;82:2743–2767.
[17] Husain MA, Tariq A, Hameed S, Arif MSB, Jain A. Comparative assessment of maximum power point tracking procedures for photovoltaic systems. Renew Sustain Energy Rev 2017;2:5–17.
[18] Pandey A, Dasgupta N, Mukerjee A. High-Performance Algorithms for Drift Avoidance and Fast Tracking in Solar MPPT System. IEEE Trans Energy Convers 2008;23:681–689.
[19] Liu F, Duan S, Liu F, Liu B, Kang Y. A Variable Step Size INC MPPT Method for PV Systems. IEEE Trans Ind Electron 2008;55:2622–2628.
[20] Mei Q, Shan M, Liu L, Guerrero JM. A Novel Improved Variable Step-Size Incremental-Resistance MPPT Method for PV Systems. IEEE Trans Ind Electron 2011;58:2427–2434.
[21] Killi M, Samanta S. Voltage-Sensor-Based MPPT for Stand-Alone PV Systems Through Voltage Reference Control. IEEE Trans. Emerg. Sel. Topics Power Electron 2019;7:1899–1407
[22] Subudhi B, Pradhan R. A New Adaptive Maximum Power Point Controller for a Photovoltaic System. IEEE Trans Sustain Energy 2019;10:1625–1632.
[23] Manoharan P, Subramaniam U, Babu T S, Padmanaban S, Nielsen J B H, Mitolo M, Ravichandaran S. Improved Perturb and Observation Maximum Power Point Tracking Technique for Solar Photovoltaic Power Generation Systems. IEEE Systems Journal 2020. (Early Access) doi: 10.1109/JSYST.2020.3003255.
[24] Abouadane H, Fakkar A, Sera D, Lashab A, Spataru S, Kerekes T. Multiple-Power-Sample Based P&O MPPT for Fast-Changing Irradiance Conditions for a Simple Implementation. IEEE J of Photovolt 2020;10:1481–1488.
[25] Gunasekaran M, Krishnasamy V, Selvam S, Almakhles D J, Norma Anglani. An Adaptive Resistance Perturbation Based MPPT Algorithm for Photovoltaic Applications. IEEE Access 2020;8:196890–196901.
[26] Satapathy S S, Kumar N. Framework of maximum power point tracking for solar PV panel using WSPS technique. IET Renew Power Gener 2020;14:1668–1676.

[27] Necaibiaa S, Kelaiaiaa M S, Labara H, Necaibiab A, Castronuovo E D. Enhanced auto-scaling incremental conductance MPPT method, implemented on low-cost microcontroller and SEPIC converter. Solar Energy 2019;180:152–168.
[28] Elobaid LM, Abdelsalam AK, Zakzouk EE. Artificial neural network-based photovoltaic maximum power point tracking techniques: a survey. IET Renew Power Gener 2015;9:1043–1063.
[29] Oshaba A S, Ali E S, Abd Elazim S M. PI controller design using ABC algorithm for MPPT of PV system supplying DC motor pump load. Neural Comput & Applic 2017;28:353–364.
[30] Oshaba A S, Ali E S, Abd Elazim S M. PI controller design for MPPT of photovoltaic system supplying SRM via BAT search algorithm. Neural Comput & Applic 2017;2:651–667.
[31] Selvakumar S, Madhusmita M, Koodalsamy C, Simon S P, Sood Y R. High-Speed Maximum Power Point Tracking Module for PV Systems. IEEE Trans Ind Electron 2019;66:1119–1129.
[32] Shams I, Mekhilef S, Tey K S. Improved Team Game Optimization Algorithm Based Solar MPPT with Fast Convergence Speed and Fast Response to Load Variations. IEEE Trans Ind Electron 2020. (Early Access) doi: 10.1109/TIE.2020.3001798.
[33] Pervez I, Shams I, Mekhilef S, Sarwar A, Tariq M, Alamri B. Most Valuable Player Algorithm based Maximum Power Point Tracking for a Partially Shaded PV Generation System. IEEE Trans Sustain Energy 2021. (Early Access) doi: 10.1109/TSTE.2021.3069262.
[34] Mohanty P, Bhuvaneswari G, Balasubramanian R, Dhaliwal NK. MATLAB based modeling to study the performance of different MPPT techniques used for solar PV system under various operating conditions. Renew Sustain Energy Rev 2014;38:581–593.
[35] Gupta A, Chauhan YK, Pachauri YK. A comparative investigation of maximum power point tracking methods for solar PV system. Solar Energy 2016;136:236–253.
[36] Andrejašič T, Jankovec M, Topič M. Comparison of direct maximum power point tracking algorithms using EN 50530 dynamic test procedure. IET Renew Power Gener 2011;5:281–286.
[37] Brito MAGD, Galotto L, Sampaio LP, Melo GDAE, Canesin CA. Evaluation of the Main MPPT Techniques for Photovoltaic Applications. IEEE Trans Ind Electron 2013;60:1156–1167.
[38] Bataineh K. Improved hybrid algorithms-based MPPT algorithm for PV system operating under severe weather conditions. IET Power Electron 2019;12:703–711.
[39] Enany M A, Farahat M A, Nasr A. Modeling and evaluation of main maximum power point tracking Algorithms for photovoltaics systems. Renew Sustain Energy Rev 2016;58:1578–1586.
[40] Ahmed J, Salam Z. An improved perturb and observe (P&O) maximum power point tracking (MPPT) algorithm for higher efficiency. Appl Energy 2015;150:97–108.
[41] Tekle, F.T.: 'Assessment of Solar Energy Resources in Ethiopia'. M.S. Thesis, Norwegian University of Science and Technology, 2014.
[42] Azzopardi B, Emmott CJM, Urbina A, Krebs FC, Mutale J, Nelson J. Economic assessment of solar electricity production from organic-based photovoltaic modules in a domestic environment. Energy Environ. Sci. 2011,4, 3741–2753.
[43] Adly M, Strunz K. Irradiance-Adaptive PV Module Integrated Converter for High Efficiency and Power Quality in Standalone and DC Microgrid Applications. IEEE Trans Ind Electron 2018;65:436–446.
[44] Drissi H, Khediri J, Zaafrane W, Braiek EB. Critical factors affecting the photovoltaic characteristic and comparative study between two maximum power point tracking algorithms. Intern J. of Hydron Energy 2016;43:8689–8702.
[45] Ram JP, Babu TS, Rajasekar N. A comprehensive review on solar PV maximum power point tracking techniques. Renew Sustain Energy Rev 2017;67:826–847.
[46] Soulatiantork P, Cristaldi L, Faifer M, Laurano C, Ottoboni R, Toscani S. A Tool for Performance Evaluation of MPPT Algorithms for Photovoltaic Systems. Measurement 2018;128:537–544.
[47] Santos OL et al. Analysis, Design, and Implementation of a Static Conductance-Based MPPT Method. IEEE Trans on Power Electron 2019; 34:1960–1979.
[48] Jesus VMRd, Cupertino AF, Xavier LS, Pereira HA, Mendes VF. Comparison of MPPT Strategies in Three-Phase Photovoltaic Inverters Applied for Harmonic Compensation. IEEE Trans Ind Appl 2019;55:5141–5152.
[49] Vicente EM, Vicente PdS, Moreno RL, Ribeiro ER. High-efficiency MPPT method based on irradiance and temperature measurements. IET Renew Power Gener 2020;14:986–995.

[50] Dadkhah J, Niroomand M. Optimization Methods of MPPT Parameters for PV Systems: Review, Classification, and Comparison. J. Mod. Power Syst. Clean Energy 2021;9:225–236.
[51] Swaminathan N, Lakshminarasamma N, Cao Y. A Fixed Zone Perturb and Observe MPPT Technique for A Standalone Distributed PV System. IEEE Trans. Emerg. Sel. Topics Power Electron 2021. (Early Access) doi: 10.1109/JESTPE.2021.3065916.
[52] Sera D, Mathe L, Kerekes T, Spataru SV, Teodorescu R. On the Perturb-and-Observe and Incremental Conductance MPPT Methods for PV Systems. IEEE J. of Photovolt 2013;3:1070–1078.
[53] Azizi A, Logerais PO, Omeiri A, et al. Impact of the aging of a photovoltaic module on the performance of a gridconnected system. Solar Energy 2018;174:445–454.
[54] Jately V, Bhattacharya S, Azzopardi B, Montgareuil A G d, Joshi J, Arora S, Voltage and Current Reference Based MPPT under Rapidly Changing Irradiance and Load Resistance. IEEE Trans. on Energy Conv 2021. (Early Access) doi: 10.1109/TEC.2021.3058454.
[55] Jately V, Arora S. Development of a dual-tracking technique for extracting maximum power from PV systems under rapidly changing environmental conditions. Energy 2017;133:557–571.
[56] Kollimalla SK, Mishra MK. Variable Perturbation Size Adaptive P&O MPPT Algorithm for Sudden Changes in Irradiance. IEEE Trans Sustain Energy 2014;5:718–728.